Ancillary Ligand Effects in Niobocene Olefin Hydride Complexes and Hydrocarbon Oxidation by Palladium(II) Complexes

Thesis by

Lily Joy Ackerman

In Partial Fulfillment of the Requirements for the

Degree of Doctor of Philosophy

Division of Chemistry and Chemical Engineering

California Institute of Technology

Pasadena, California

2003

(Defended May 14, 2003)

For Victor, My Family, the SD crowd, and Kendra

Acknowledgements

There are many people I must thank who have helped me in some way during my graduate career both scientifically and emotionally. First, I must thank John Bercaw for his continuous support and encouragement throughout my career. John, you have given me unique opportunities to grow as a scientist and a person, and I have often thought of you and Diane as my "surrogate parents." Thank you for caring about me beyond the role of research advisor.

I have been very fortunate to interact with other individuals who I would also consider as research advisors. Jay Labinger has been extremely helpful whenever I have interacted with him. Thank you Jay for always taking the time to answer my questions and for helpful advice when I needed it. Malcolm and Jenny Green, my U.K. advisors, are just awesome. Thank you Malcolm and Jenny for allowing me to work in your labs at Oxford. Although I was only at the ICL for a short time, you both have treated me as if I was another one of your students. Your kind words have given me more confidence in myself especially when I needed it. Also thanks to Nick Rees at Oxford for teaching me the subtleties of NMR.

My Ph.D. committee is the best ever! Thank you to Bob Grubbs, Brian Stoltz, and Harry Gray for reading my proposals and thesis and for teaching me a lot. I admire the way all three of you have helped me learn and think about chemistry in my exams in a very constructive way. A special thanks to Harry, for inspiring me during three years of your 2nd term, Friday morning class, where I really learned something about inorganic chemistry. Also, thanks Harry, for being my friend and for listening to both my joys and woes.

What can I say about the Bercaw Group? Without you all, my years at Caltech would not have been filled with wild and crazy moments. Susan Schofer, you have been my best friend in the group almost since the beginning. I am going to really miss you and all of our long discussions outside of Noyes in various secret hiding places. Thanks for always taking the time to talk to me and for keeping me sane. I hope we continue to have great discussions in the future, maybe even in Europe! The current Bercaw group members have made the last few years unforgettable. It seems that each Christmas Party has gotten crazier

than the previous, culminating in gangsta rap karaoke, overturned water coolers, and a black eye in 2002. But 2001 was *not too shabby*, especially with Gerry getting wasted by the hoods in 209. Dave Weinberg has provided *good times* on many occasions with Big Fizz in tow. Dave's partner in crime, Theo Agapie, has been a great labmate and friend. Theo, I have great memories of dealing with cranes and dryboxes, putting out fires, and hanging out at the Pasadena DMV with you. The Famous Theo and Dave Candidacy Experience also made me feel like I wasn't alone when I was struggling to write my props and thesis. Thank you to Parisa Merhkodavandi and Heather Weincko for hanging out with me at Bercaw Bulls games. The Bercaw Bulls underwent a remarkable transformation in 2003 due to the basketball savvy of our coach, Jeff Byers. Jeff, your spirit and ability to have fun on the court inspire me. Thanks to Jonathan Owen for your enthusiasm for chemistry; it definitely helped keep me excited. Cliff Baar and Alan Heyduk both have shared their chemistry expertise with me. I truly appreciated Cliff's unique personality, and thanks Alan for always helping me with experiments and chemistry questions. I have two fun classmates, Endy Min and Sara Klamo. Endy, thank you for being kind and understanding person to talk to. A special thanks to Sara, for great chemistry discussions with me back in the nook, for being my TA buddy during Chem 112, for helping me understand Chem 153, and for hanging out behind the green box with me for hours!

The Bercaw Group members who have left during my stay have been greatly missed. There was a time when the south side of Noyes 209 was the place to be thanks to Alex Muci, Chris "Theory" Brandow, Seva Rostovtsev, and Joseph Sadighi. I have learned so much chemistry from each of you. Thanks Alex for supporting me and always being my friend. Thanks Theory for giving me a shoulder to lean on and for sharing your thoughts about life with me. Thanks Annita for helping me learn platinum chemistry; we also had a lot of fun in my little red car during your driving lessons. Graduate students Jeff Yoder, Steve Miller, Paul Chirik, Deanna Zubris and Postdocs Ola Wendt, John Scollard, and Chris Levy all helped me get started in lab in the very beginning. Thank you Paul and Deanna for sharing the Group 5 project with me and for helping me get started with what resulted in a substantial part of my thesis. A special thanks to Ola and Jeff for spending a lot of time explaining chemistry and especially NMR

to me. Also, thanks to Christoph Balzarek for being another great 209 labmate. Thank you to Antek Wong-Foy for always being willing to help anyone out, in lab or as a friend. Thanks Antek for helping me when I needed it most.

My friends in San Diego, Leslie Wilkins, Ryan Daniels, Jess Dalisay, Johnny Schneller, and Jenny and Dave Blood, have provided me with the most fun LA getaway party place one could ever hope for. Thank you guys for all of your support and for sticking by me throughout this California adventure. I couldn't have done it without all of you; you are my more than my friends, but also my family. I have always felt like I had a home at the apartment building on Narragansett where we have had so many good times with wigs, tattoos (go star tattoo gang!), Muad'Dib, hanging in OB, going to shows, or just getting wasted! Although I won't be as close by, our adventures together have just begun!

Thank you, Kendra Spivey, for continuing to be my best friend even though I have been across the country and even across the ocean. You have put up with late night phone calls when I have been freaking out. I especially appreciate all of the times I called you from England as I stood in the lonely, red phone booths. You have been my strength when I was the most desperate. I love ya, girl! My parents, Ron and Nga Ackerman, and my sister and family, Kim, John, and Auggie (Gus) Koepke have also been very supportive throughout my graduate career. Thank you all for putting up with my ups and downs. Also, this Ph.D. would not have been possible without the help and support of others at Caltech. Thanks to Pat Anderson and Dian Buchness for help and patience; to Larry Henling for all of the time you put into my crystal structures; to Paul Carroad, Chris Smith, and Steve Gould for keeping the department running; to Angelo DiBilio for your help with the EPR; to Scott Ross for NMR assistance; and of course to Rick Gerhart for your amazing glass blowing abilities. Also, thanks to Raissa Trend for being a good friend this past year.

Finally, I must thank the love of my life, Victor Rucker. Babe, we've come a long way, and I hope we continue to love and care for each other forever. Thank you for understanding me perhaps better than anyone else, and for sticking by me through all of the tough times. We are about to embark on one of the biggest adventures of our lives as we leave Caltech with our Ph.D.'s (finally!). I love you meeps, and I couldn't have made it without you.

Abstract

To examine the effects of cyclopentadienyl and olefin substitution on preferred stereochemistry, the preparation of a series of singly [$SiMe_2$]-bridged *ansa*-niobocene olefin hydride complexes is described. These complexes serve as stable transition state analogues for the much more kinetically labile group 4 metallocenium cationic intermediates in metallocene-catalyzed olefin polymerization. Characterization of the thermodynamically preferred isomers of niobocene olefin hydride complexes reveals that placement of a single alkyl substituent on the cyclopentadienyl ligand array may have a moderate effect on the stereochemistry of olefin coordination.

Using dynamic NMR methods the rates of hydrogen exchange following intramolecular ethylene insertion into the metal–hydride bond have been measured for singly and doubly bridged group 5 *ansa*-metallocene complexes. The singly bridged *ansa*-niobocenes exchange up to 3 orders of magnitude faster than unbridged complexes. However, the doubly bridged *ansa*-tantalocene complex exchanges at a rate comparable to that previously reported for the unlinked and much slower than a singly bridged complex. These "*ansa*-effects" were investigated by DFT calculations on model complexes. The computed exchange pathway showed the presence of an agostic ethyl intermediate. The calculated barriers for hydrogen exchange of model unbridged, singly bridged, and doubly bridged niobocenes correlate with the experimental results.

N,*N*'-Diaryl-α-diimine-ligated Pd(II) dimethyl complexes undergo protonolysis with HBF_4 (aq) in trifluoroethanol (TFE) to form the cationic complexes [(α-diimine)Pd(CH_3)(H_2O)][BF_4]. The cations activate benzene C–H

bonds at room temperature. Kinetic analyses reveal trends similar to those observed for the analogous Pt complexes: the C–H activation step is rate determining and is inhibited by H_2O, which is consistent with a mechanism in which benzene substitution proceeds by a solvent- (TFE-) assisted associative pathway. After benzene C–H activation under 1 atm O_2, the products of the reaction are biphenyl and a dimeric μ-hydroxide complex, $[(\alpha\text{-diimine})Pd(OH)]_2[BF_4]_2$. The Pd(0) formed in the reaction is reoxidized by O_2 after the oxidative C–C bond formation. Toluene and α,α,α-trifluorotoluene were investigated as substrates to examine the regioselectivity of arene coupling.

TABLE OF CONTENTS

List of Figures and Tables

Chapter 1

Chapter 2

Chapter 3

Chapter 1

Preparation of *ansa*-Niobocene Olefin Hydride Complexes as Transition State Analogues in Metallocene-Catalyzed Olefin Polymerization

The text of this chapter was taken in part from the following manuscript:

Chirik, P. J.; Zubris, D. L.; Ackerman, L. J.; Henling, L. M.; Day, M. W.; Bercaw, J. E. *Organometallics* **2003**, *22*, 172-187.

Abstract

To examine the effects of cyclopentadienyl and olefin substitution on preferred stereochemistry, a series of singly [$SiMe_2$]-bridged *ansa*-niobocene olefin hydride complexes has been prepared via reduction and alkylation of the corresponding dichloride complexes. In this manner, [$Me_2Si(\eta^5\text{-}C_5H_4)(\eta^5\text{-}C_5H_3\text{-}3\text{-}R)$]$Nb(CH_2{=}CHR')H$ (R = $CHMe_2$, CMe_3; R' = H, C_6H_5), and *rac*- and *meso*-[$Me_2Si(\eta^5\text{-}C_5H_3\text{-}3\text{-}R)(\eta^5\text{-}C_5H_3\text{-}3\text{-}R)$]$Nb(CH_2{=}CH_2)H$ (R = CMe_3) have been prepared and characterized by NMR spectroscopy and in some cases, X-ray diffraction. These compounds serve as stable transition state analogues for the much more kinetically labile group 4 metallocenium cationic intermediates in metallocene-catalyzed olefin polymerization. Characterization of the thermodynamically preferred isomers of niobocene olefin hydride complexes reveals that placement of a single alkyl substituent on the cyclopentadienyl ligand array may have a moderate effect on the stereochemistry of olefin coordination.

Introduction

Stereospecific olefin polymerization promoted by group 3 and 4 *ansa*-metallocene catalysts represents one of the most enantioselective chemical transformations known.[1] Elucidation of the steric and electronic factors that control this remarkable selectivity may aid in the design of new catalysts and also result in the development of new asymmetric transformations. Considerable effort has been devoted toward understanding the nature of the transition state for the C–C bond forming step with metallocene polymerization catalysts. The electronic requirements for an active catalyst are fairly well accepted: a metallocene alkyl with two vacant orbitals (Chart 1), where one orbital is used to accommodate the incoming olefin while the other allows for α-agostic assistance[2] in the transition state for carbon-carbon bond formation.[3]

Chart 1

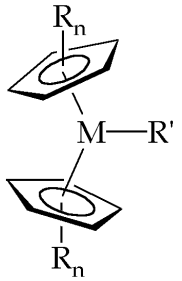

M = Sc, Y, lanthanide
R' = hydride or alkyl

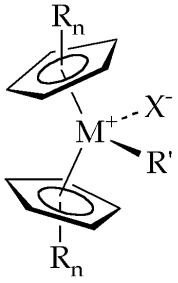

M = Ti, Zr, Hf
R' = hydride or alkyl
X^- = weakly coordinating anion

Understanding the key steric interactions in the olefin insertion transition state has also been the focus of many experimental and theoretical investigations. Calculations by Corradini[4] demonstrate that the enantiofacial approach of the olefin is determined by the orientation of the metal alkyl unit, such that the olefin

substituent is placed in a trans relationship with the β-carbon of the metal polymeryl unit. The polymeryl is believed to orient toward the most open portion of the metallocene framework (Scheme 1; schematic view of C_2-symmetric metallocene looking into the wedge). The first experimental evidence in support of this model was provided by Pino.[5] Hydrooligomerization

Scheme 1

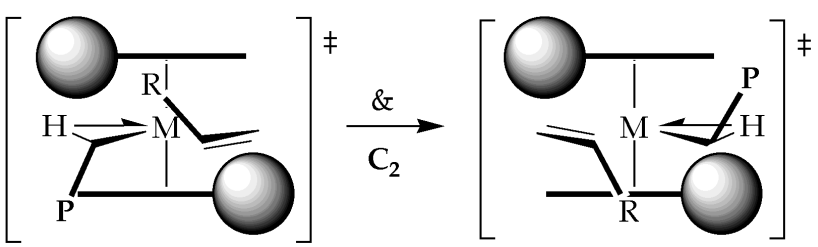

of α-olefins with optically pure [ethylenebis(4,5,6,7-tetrahydroindenyl)]-zirconium dichloride (EBTHIZrCl_2) produced chiral hydrotrimers and hydrotetramers with the predicted absolute configurations.[6] In contrast to polymerizations/oligomerizations, deuteriations of α-olefins such as styrene and pentene produced lower ee's with the opposite enantiofacial selectivity.[7] Similarly, work from our laboratories defined the diastereoselective transition structures for 1-pentene addition to yttrium–hydride and yttrium–pentyl bonds.[8] An optically pure, isotopically chiral 1-pentene was prepared and used to evaluate the stereoselectivity with an optically pure yttrocene. The absolute diastereoselectivities were established: insertion into yttrium–hydride bond proceeds with modest selectivity (34% ee); insertion into yttrium–pentyl bond proceeds via the other diastereomeric transition state with very high levels (> 95% ee) of selectivity. Analogous transition state arguments have been proposed

for the titanocene-catalyzed asymmetric hydrogenation of olefins reported by Buchwald and co-workers.[9]

The stereochemical model developed in the C_2-symmetric isospecific systems has since been extended to include C_s-symmetric syndiospecific catalysts.[10] The favored transition state geometry for syndiospecific catalysts is shown in Scheme 2 (schematic view of a C_s-symmetric metallocene looking into the wedge), where again the dominant stereo-directing interaction is a trans relationship between propylene methyl and the C_α–C_β bond of the polymer chain. Whether on the left or right side of the metallocene wedge, the growing polymer chain extends up and away from the more sterically demanding cyclopentadienyl moiety, thus forcing the propylene methyl group down. In syndiospecific catalysts, this lower cyclopentadienyl ligand contains an open region to accommodate the methyl substituent on the incoming monomer. Essential to the stereospecificity is a regular alternation of propylene approach from one side of the metallocene wedge and then the other.[11]

Scheme 2

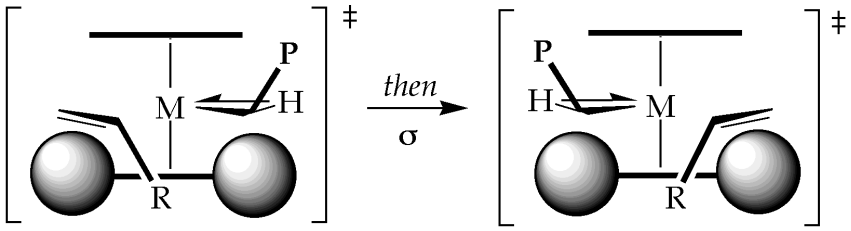

Although these stereochemical models have been quite successful in explaining the high levels of stereocontrol observed with C_2- and C_s-symmetric catalysts, the stereospecificity of some metallocene catalysts cannot be readily rationalized. For example, the C_1-symmetric, monosubstituted, singly

silylene-bridged zirconocene [$Me_2Si(\eta^5\text{-}C_5H_4)(\eta^5\text{-}C_5H_3\text{-}3\text{-}R)$]$ZrCl_2$/MAO (R = CMe_3, $CHMe_2$), originally reported by Miya,[12a] polymerizes propylene with [*mmmm*] contents exceeding 70% (Scheme 3). Obviously, the stereocontrol mechanisms of Schemes 1 and 2 do not apply, and thus one cannot readily explain such high isospecificity.

Scheme 3

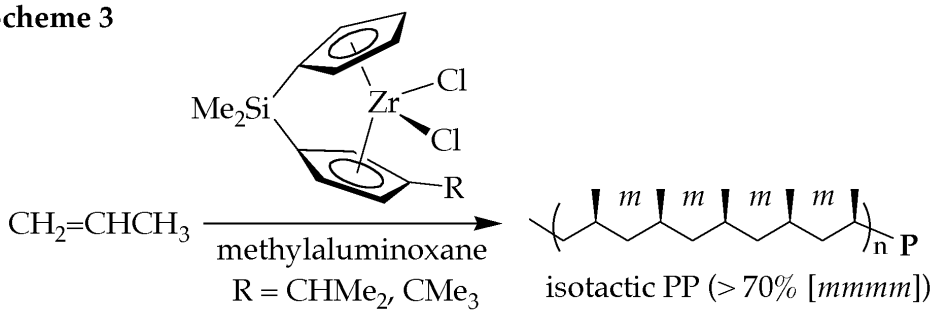

A possible approach to understanding the stereochemistry of olefin insertion would be to model the carbon-hydrogen or carbon-carbon bond-forming transition states of a group 4 metallocene catalyst using the *ground-state analogue*, a (stable) group 5 (M = Nb, Ta) metallocene olefin hydride or olefin alkyl complex. These complexes have been used to investigate the steric and electronic effects for olefin insertion into metal–hydride bonds with *bis*(cyclopentadienyl) and related *ansa*-niobocene and -tantalocene olefin hydride complexes.[13] The niobocene and tantalocene complexes are formally M(III), d^2 metal centers (Scheme 4) that stabilize the olefin–metal bond through a strong π-back-bonding interaction.

Conventional NMR and X-ray diffraction experiments may be used to determine the structure of the metallocenes and thus to establish the direction and magnitude of steric effects (shown for one of the enantiomers of

{[$Me_2Si(\eta^5\text{-}C_5H_4)(\eta^5\text{-}C_5H_3\text{-}3\text{-}R^1)$]M} in Chart 2). There are three stereoisomeric relationships between the olefin hydride complexes: (1) the preference for the

Scheme 4

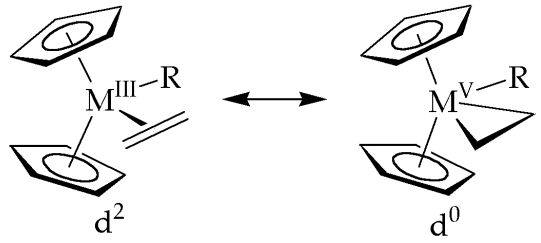

(M = Nb, Ta; R = H, alkyl)

olefin to be on the side of the metallocene wedge distal or proximal to the cyclopentadienyl substituent R^1, (2) the preference for olefin coordination with its substituent R^3 syn or anti to the substituted cyclopentadienyl ring and (3) the preference for the olefin substituent R^3 to position itself endo or exo relative to the metallocene hydride or metallocene alkyl fragment R^2.

Chart 2

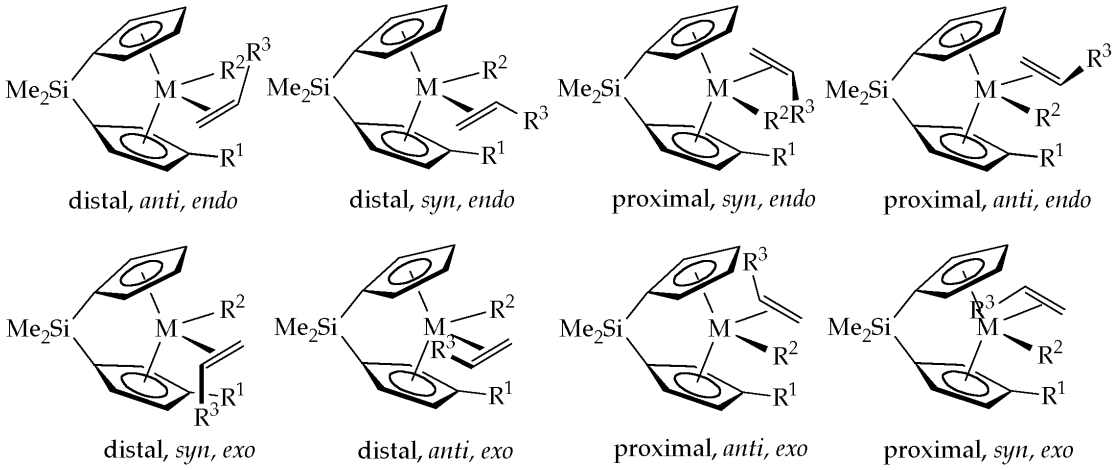

(M = Nb, Ta; R^1, R^3 = alkyl; R^2 = H, alkyl)

Reports of group 5 *ansa*-metallocenes are limited and generally restricted to C_{2v}-symmetric metallocene frameworks,[14,15ab,16,17,18] except for one report of

C_1-symmetric *ansa*-niobocene imido complexes.[17c] In this report we describe the synthesis and characterization of a series of low-symmetry, singly [$SiMe_2$]-bridged niobocene olefin hydride complexes. The preferred structures of these complexes have been examined regarding the important stereodirecting interactions between the coordinated olefin and the cyclopentadienyl ligand substituents. These olefin hydride complexes are potential precursors for the preparation of olefin alkyl complexes. Using these structures as transition state analogues, we hope to gain some insight into the basis of stereoselectivity for propylene polymerizations with group 4 metallocene catalysts.

Results and Discussion

Preparation of Singly [$SiMe_2$]-Bridged Olefin Hydride Complexes.

The synthetic strategy for the preparation of group 5 *ansa*-metallocene olefin hydride complexes is based upon the methodology developed for unlinked metallocene complexes. Essential to the synthesis is a convenient route to the corresponding group 5 metallocene dichloride complex, which in turn may be simultaneously reduced and alkylated via addition of an excess of the appropriate Grignard reagent (Scheme 5).

Scheme 5

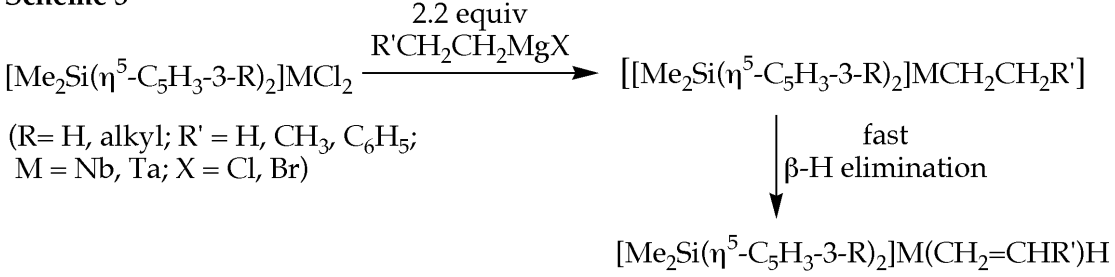

Preparation of *ansa*-niobocene dichloride complexes is accomplished by extension of previously reported synthetic protocols. Metalation of singly [$SiMe_2$]-bridged cyclopentadienyl ligands proceeds via addition of the dilithio salt of the ligand to a slurry of $NbCl_4(THF)_2$ in diethyl ether.[17a] In this manner, [$Me_2Si(\eta^5\text{-}C_5H_4)(\eta^5\text{-}C_5H_3\text{-}3\text{-}CHMe_2)$]$NbCl_2$ (iPrSpNbCl$_2$, **1**); [$Me_2Si(\eta^5\text{-}C_5H_4)(\eta^5\text{-}C_5H_3\text{-}3\text{-}CMe_3)$]$NbCl_2$ (tBuSpNbCl$_2$, **2**) and [$Me_2Si(\eta^5\text{-}C_5H_3\text{-}3\text{-}CMe_3)_2$]$NbCl_2$ (DpNbCl$_2$, **3**) have been prepared (eq 1). Each

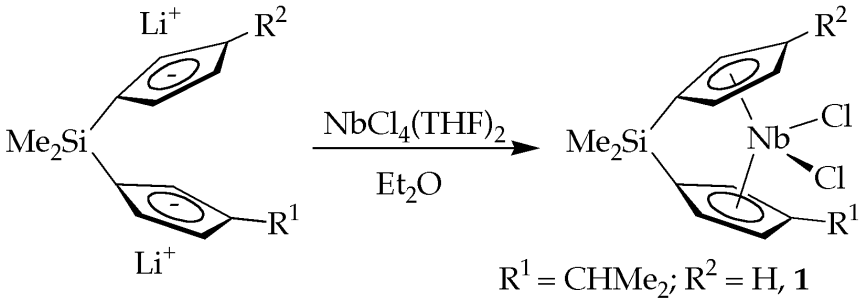

(1)

$R^1 = CHMe_2$; $R^2 = H$, **1**
$R^1 = CMe_3$; $R^2 = H$, **2**
$R^1 = R^2 = CMe_3$, **3** (*meso* and *racemic* isomers)

dichloride complex is first extracted into CH_2Cl_2 to remove LiCl. This purification is satisfactory for **1**, but further purification is necessary for **2** and **3**. Complex **2** is isolated after sublimation at 160 ˚C. Complex **3** is obtained as a mixture of racemic and meso isomers (vide infra), and this mixture is isolated after a second extraction into petroleum ether. Characterization of the paramagnetic Nb(IV) dichloride complexes has been accomplished by ambient-temperature EPR spectroscopy and by elemental analysis. The EPR spectra for **1** - **3** display 10-line patterns indicative of a single electron localized on a Nb(IV) center (^{93}Nb = 100%, S = 9/2).

Addition of 2.2 equiv of CH_3CH_2MgBr to **1** in diethyl ether results in formation of the ethylene hydride complex, iPrSpNb(η^2-CH_2CH_2)H (**4**) (eq 2).

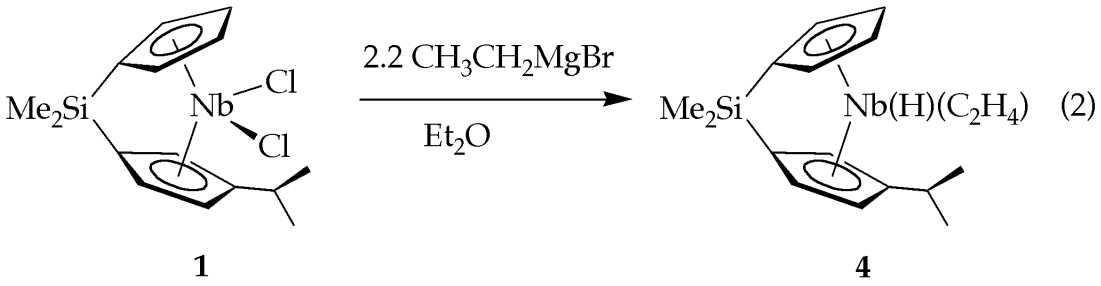

(2)

1 **4**

^{1}H NMR spectroscopy reveals that, of the two possible ethylene hydride isomers, one isomer is formed preferentially in a 95:5 ratio. A diagnostic upfield metal hydride resonance is observed at -2.60 ppm for **4**. The ^{1}H NMR spectrum for **4** at 25 ˚C contains broad resonances for the niobium hydride and for the coordinated ethylene, indicative of rapid and reversible olefin insertion and β-hydrogen elimination.[13]

Structural assignment of the predominant ethylene hydride isomer for **4** has been accomplished with NOE difference NMR spectroscopy.[19] Irradiation of the metal hydride affords a strong NOE enhancement in the isopropyl methine, isopropyl methyl groups, and the *endo*-ethylene protons. Likewise, irradiation of the isopropyl methine results in enhancement in the metal hydride resonance. No enhancement in any ethylene peaks is observed. These data, taken together with more subtle cyclopentadienyl and [$SiMe_2$] NOE enhancements, allow the assignment of the major isomer. The ethylene is coordinated in the more open portion of the metallocene wedge, away from the isopropyl substituent (i.e., the distal isomer). The formation of predominantly

one ethylene hydride isomer (95%) demonstrates the moderate stereodirecting ability of a monosubstituted *ansa*-metallocene.

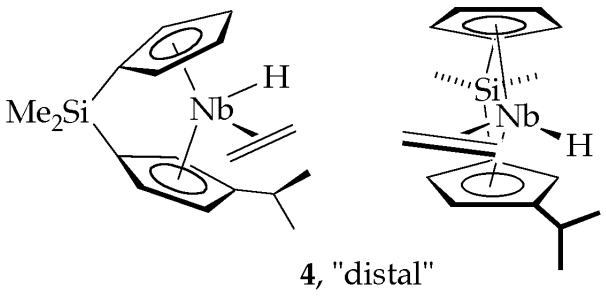

4, "distal"

Addition of CH_3CH_2MgBr to **2** affords the *ansa*-niobocene ethylene hydride complex tBuSpNb(η^2-CH_2CH_2)H (**5**) in modest yield (eq 3). Only one isomer is observed by ^1H NMR spectroscopy. Slow cooling of a petroleum ether

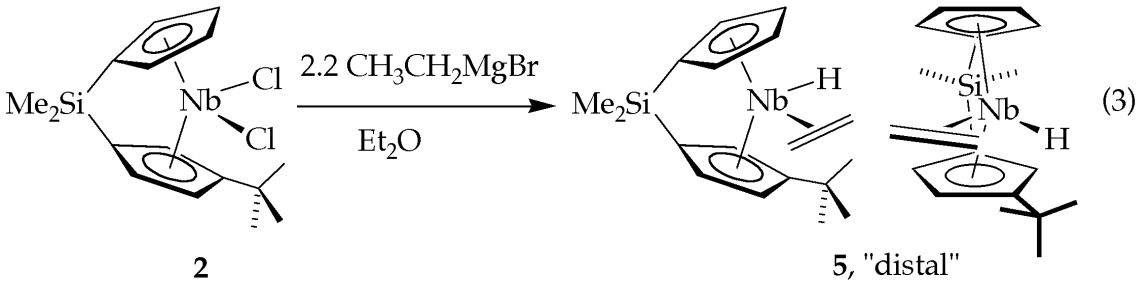

2 **5**, "distal" (3)

solution of **5** affords yellow crystals suitable for X-ray diffraction. The solid-state structure of **5** is shown in Figure 1 and reveals that the ethylene ligand is coordinated in the open portion of the metallocene wedge away from the *tert*-butyl substituent. The niobium hydride was located in a difference map, and the Nb–H bond length was refined to 1.68(2) Å. The C(17)-C(18) bond distance of 1.411(2) Å is consistent with other group 5 olefin adducts, indicative of substantial metallocyclopropane character.[20]

Reaction of complex **3** with CH_3CH_2MgBr results in a mixture of two isomers in a 50:50 ratio. The number of cyclopentadienyl resonances in the ^1H

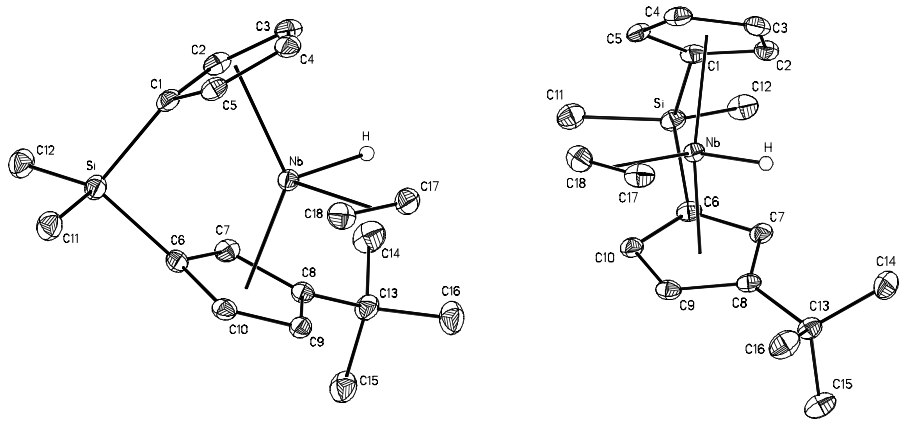

Figure 1. Molecular structure of **5** with 50% probability ellipsoids. Hydrogen atoms (other than hydride shown at arbitrary scale) have been omitted.

NMR indicate that one isomer is of C_s-symmetry, *meso*-DpNb(η^2-CH_2CH_2)H (**6a**); the other isomer, *rac*-DpNb(η^2-CH_2CH_2)H (**6b**), is C_1-symmetric. The isomers **6a** and **6b** can be separated by fractional recrystallization from cold petroleum ether. NOE difference experiments for the *meso* isomer **6a** indicate that the ethylene is coordinated away from the *tert*-butyl substituents (eq 4).

Preparation of *ansa*-niobocene complexes with α-olefins is accomplished via addition of the appropriate Grignard reagent to the dichloride complexes. Addition of 2.2 equiv of $C_6H_5CH_2CH_2MgCl$ to an ethereal solution of **1** affords the styrene hydride complex iPrSpNb(η^2-$CH_2CHC_6H_5$)H (**7**, eq 5). Three isomers are formed in a 53:38:9 ratio for **7** (major:minor:trace isomers).

Analysis of the product mixture by NOE difference ^1H NMR spectroscopy allows assignment of the major and minor styrene hydride complexes.

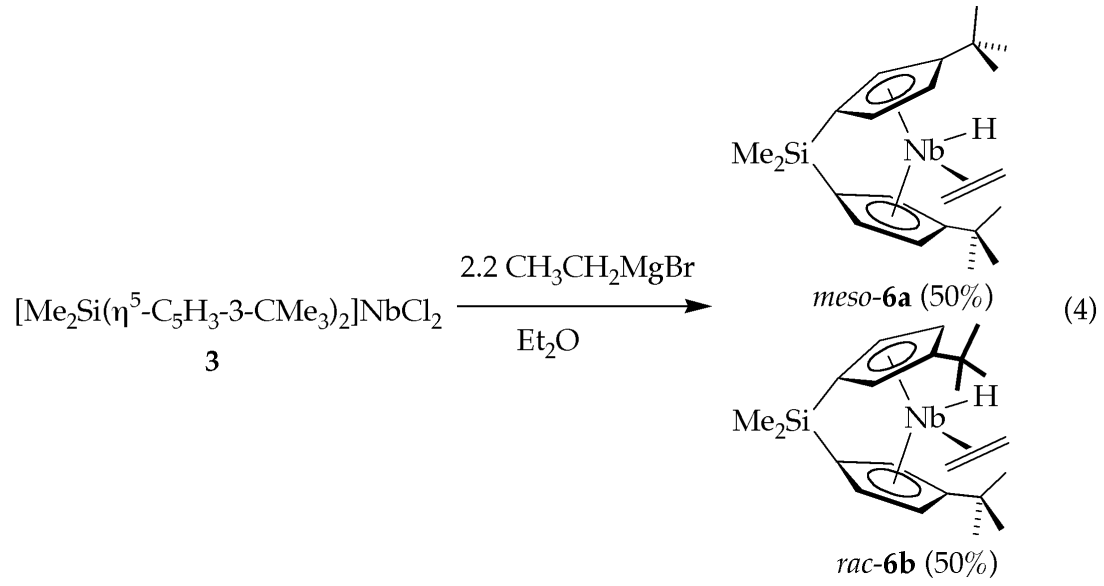

(4)

Irradiation of the metal hydride resonance results in strong NOE enhancements in the isopropyl substituent, one olefinic styrene resonance, and the ortho hydrogens of the phenyl ring. Likewise, irradiation of the isopropyl substituent results in no enhancement of the styrene protons. These data indicate that for the major isomer, the styrene is coordinated anti to the isopropyl substituents and in

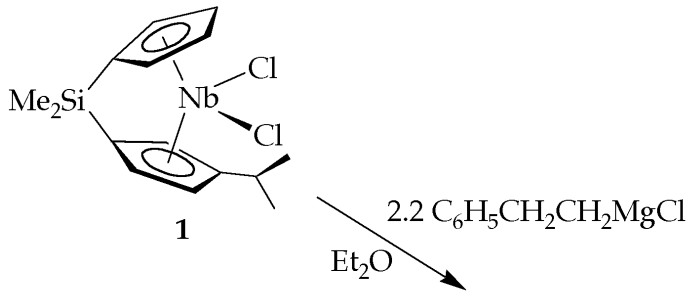

[Me2Si(η5-C5H4)(η5-C5H3-3-CHMe2)]Nb(CH2=CHC6H5)H, **7** (5)

an endo fashion, where the phenyl ring is directed toward the interior of the metallocene wedge. Presumably unfavorable steric interactions between the phenyl ring and the [Me_2Si] linker discourage formation of exo isomers that were

observed with unlinked niobocene and tantalocene styrene hydride complexes.[15ab]

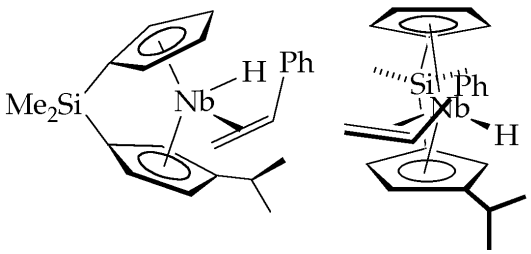

7a: distal, *anti*, *endo* (53%)

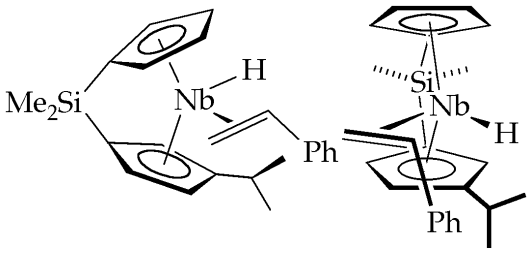

7b: distal, *syn*, *endo* (38%)

Differentiation between the enantiofacial preference of styrene hydride isomers has been obtained from more subtle NOE enhancements between the cyclopentadienyl, dimethylsilylene, and styrene hydrogens. For **7** the major styrene hydride isomer is the one for which the phenyl ring is directed away from the isopropyl substituent, whereas in the minor isomer, the phenyl ring is directed toward the isopropyl group, with the diastereoselectivity for olefin coordination for **7** being approximately 15%. A small enantiofacial differentiation was also noted for insertion of 1-pentene into the Y–H bond of a C_2-symmetric yttrocene catalyst and for α-olefin deuteriations.[9,10] Although the enantiofacial preference for olefin coordination is poor, the site selectivity is quite good, where for **7** approximately 90% of the styrene coordination occurs with phenyl away from the isopropyl substituent, i.e., "distally."[21]

Alkylation of **2** with $C_6H_5CH_2CH_2MgCl$ in diethyl ether affords two isomers of tBuSpNb(η^2-CH_2CHPh)H, **8**, in a 90:10 ratio (eq 6). Slow cooling of a petroleum ether solution of **8** provides yellow crystals (major isomer, **8a**) suitable for X-ray diffraction analysis, as shown in Figure 2. The solid-state structure reveals that the preferred isomer has the styrene coordinated in an endo fashion

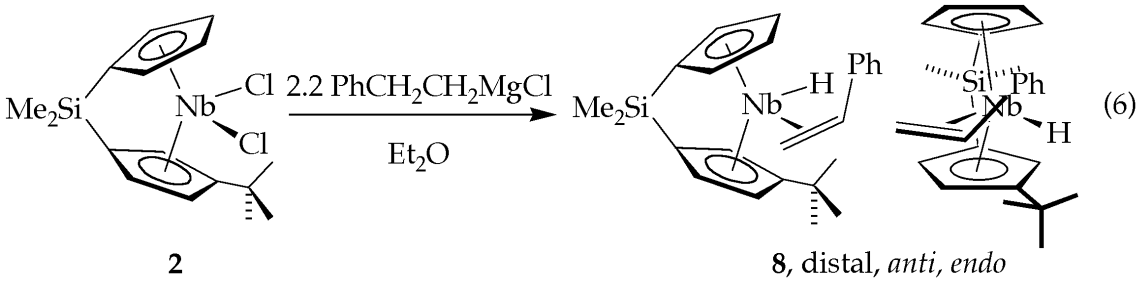

2 **8**, distal, *anti, endo*

in the open portion of the metallocene wedge with the phenyl group directed anti to the *tert*-butyl substituent. The Nb–H was located in a difference map; the distance was refined to 1.70(2) Å. The phenyl ring exhibits a modest 3.2° twist with respect to the olefinic plane. The C(17)-C(18) bond distance of 1.418(3) Å is similar to that of the complexes described herein and elsewhere.[22] Thus, a *tert*-

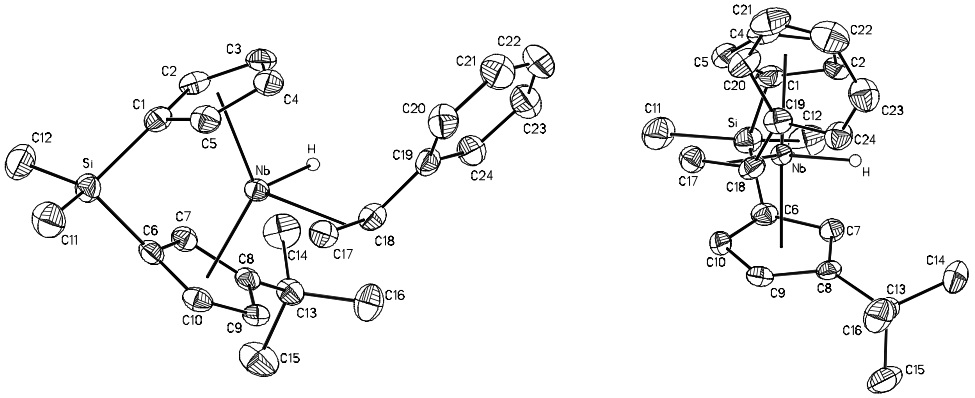

Figure 2. Molecular structure of **8a** with 50% probability ellipsoids. Hydrogen atoms (other than hydride shown at arbitrary scale) have been omitted.

butyl substituent more strongly enforces the enantiofacial preference for olefin coordination than an isopropyl substituent. It is interesting to note that lower isospecificity was observed for propylene polymerizations with iPrSpZrCl$_2$/MAO as compared with tBuSpZrCl$_2$/MAO (ca. 75% vs 85% [*mmmm*], respectively).[12b]

Conclusions

A series of singly [$SiMe_2$]-bridged *ansa*-niobocene olefin hydride complexes have been prepared via reduction and alkylation of the corresponding niobocene dichloride complexes. Their geometries have been determined in solution by NOE difference NMR spectroscopy, and in several cases the solid-state structures have been established by X-ray diffraction. Monosubstitution of the cyclopentadienyl framework with an isopropyl or *tert*-butyl group ([$Me_2Si(\eta^5\text{-}C_5H_4)(\eta^5\text{-}C_5H_3\text{-}3\text{-}R)$]Nb(olefin)H; R = $CHMe_2$, CMe_3) directs ethylene coordination such that the olefin is distal from R, ca. 20:1 for isopropyl and >50:1 for *tert*-butyl. The methyl groups of the [$SiMe_2$] linker force α-olefins such as propylene and styrene to coordinate with the olefin substituent directed toward the hydride ligand (endo), unlike the "parent" [$(\eta^5\text{-}C_5H_5)_2M$] olefin hydride complexes, for which approximately equal amounts of endo and exo isomers are obtained for the propylene and styrene hydrides. As for the ethylene hydride complexes, distal coordination of α-olefins is preferred; however, neither isopropyl nor *tert*-butyl substitution of one cyclopentadienyl ligand enforces a strong enantiofacial preference for olefin coordination for the niobium olefin hydrides.

Thus, the placement of a single isopropyl or *tert*-butyl substituent on a cyclopentadienyl ligand of [$Me_2Si(\eta^5\text{-}C_5H_4)(\eta^5\text{-}C_5H_3\text{-}3\text{-}R)$]Nb(olefin)H has a modest effect in directing the olefin coordination geometry. It would, of course, be of interest to establish the stereodirecting effects of these substituents on the conformations of the M–R' group for the corresponding

[$Me_2Si(\eta^5\text{-}C_5H_4)(\eta^5\text{-}C_5H_3\text{-}3\text{-}R)$]M(olefin)R' complexes, particularly for those metal alkyls that mimic the polymeryl groups during propylene polymerization, e.g., [M-$CH_2CH(CH_3)CH_2CHMe_2$], since it has been established that the

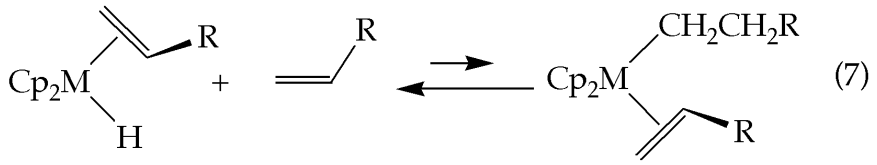

(7)

interactions of the olefin substituents with the polymeryl group are greater than with the ligand substituents (vide supra). Unfortunately, all attempts to induce olefin insertion and olefin coordinative trapping of the resultant alkyls using these *ansa*-olefin hydrides were unsuccessful. Presumably, the equilibrium needed to provide such olefin alkyls (eq 7) lies too far to the left, even for α-olefins.

Experimental

General Considerations. All air- and moisture-sensitive compounds were manipulated using standard vacuum line, Schlenk, or cannula techniques or in a drybox under a nitrogen atmosphere as described previously.[23] Argon, dinitrogen, and dihydrogen gases were purified by passage over columns of MnO on vermiculite and activated molecular sieves. Toluene and petroleum ether were distilled from sodium and stored under vacuum over titanocene.[24] Tetrahydrofuran, dimethoxyethane, and ether were distilled from sodium benzophenone ketyl. $NbCl_4(THF)_2$, 3.0 M CH_3CH_2MgBr in diethyl ether, and 1.0

M $PhCH_2CH_2MgCl$ in THF were purchased from Aldrich and used as received. All dilithio salts of ligands were prepared according to standard procedures.[25]

NMR spectra were recorded on a JEOL GX-400 (^1H, 399.78 MHz, ^{13}C, 100.53 MHz) or a Varian Inova 500 (^1H, 500.13 MHz, ^{13}C, 125.77 MHz). All chemical shifts are relative to TMS for ^1H (residual) and ^{13}C (solvent as a secondary standard). Nuclear Overhauser difference experiments were carried out on a Varian Inova 500 MHz spectrometer. Elemental analyses were carried out at the Caltech Analytical Facility by Fenton Harvey or by Midwest Microlab, Indianapolis, IN.

$[Me_2Si(\eta^5\text{-}C_5H_4)(\eta^5\text{-}C_5H_3\text{-}3\text{-}CHMe_2)]NbCl_2$ (1). In the dry box, 6.23 g (16.4 mmol) $NbCl_4(THF)_2$ and 4.00 g (16.4 mmol) of $Li_2[Me_2Si(\eta^5\text{-}C_5H_4)(\eta^5\text{-}C_5H_3\text{-}3\text{-}CHMe_2)]$ were combined in a 300 mL round-bottom flask. On the vacuum line, 175 mL Et_2O was added by vacuum transfer. The reaction was stirred overnight. The Et_2O was removed in vacuo leaving a light brown powder. The product was isolated by dissolving the crude mixture in 100 mL of CH_2Cl_2 followed by filtration of the LiCl. The CH_2Cl_2 was removed in vacuo, leaving 5.63 g (87.2%) of a dark brown solid identified as **1**. Anal. Calcd for $Nb_1Si_1C_{15}H_{20}Cl_2$ C, 46.05%, H, 4.90%; Found C, 46.04%; H, 4.97%. EPR (CH_2Cl_2): $g_{iso} = 2.01$; $a_{iso} = 99.0$ G.

$[Me_2Si(\eta^5\text{-}C_5H_4)(\eta^5\text{-}C_5H_3\text{-}3\text{-}CMe_3)]NbCl_2$ (2). This compound was prepared in a manner analogous to that for **1**, employing 1.00 g (3.91 mmol) of $Li_2[Me_2Si(\eta^5\text{-}C_5H_4)(\eta^5\text{-}C_5H_3\text{-}3\text{-}CMe_3)]$ and 1.48 g of $NbCl_4(THF)_2$ (3.91 mmol),

to afford 1.20 g (75.9%) of a dark brown solid identified as **2**. The isolated solid was sublimed, leaving 0.276 g (17.5%) of product. Anal. Calcd for $Nb_1Si_1C_{16}H_{22}Cl_2$ C, 47.30%, H, 5.35%; Found C, 46.88%; H, 5.46%. EPR (CH_2Cl_2): g_{iso} = 2.00; a_{iso} = 103.8 G.

[$Me_2Si(\eta^5$-C_5H_3-3-$CMe_3)_2$]$NbCl_2$ (3). This compound was prepared in a manner analogous to that for **1**, employing 3.00 g (9.60 mmol) of $Li_2[Me_2Si(\eta^5$-C_5H_3-3-$CMe_3)_2]$ and 3.64 g of $NbCl_4(THF)_2$ (9.60 mmol), to afford a dark brown solid identified as **3**. The isolated solid was further purified by extraction into petroleum ether. The solvent was removed leaving 1.26 g (28.4%) of product. Anal. Calcd. for $Nb_1Si_1C_{20}H_{30}Cl_2$: C, 52.00; H, 6.54. Found C, 52.42; H, 6.79. EPR (CH_2Cl_2): g_{iso} = 2.00; a_{iso} = 103.8 G.

[$Me_2Si(\eta^5$-$C_5H_4)(\eta^5$-C_5H_2-3-$CHMe_2)$]$Nb(\eta^2$-$CH_2CH_2)H$ (4ab). In the drybox, a fine swivel frit assembly was charged with 1.50 g (3.824 mmol) **1**. On the vacuum line, approximately 25 mL of dimethoxyethane was added by vacuum transfer. At -80 ˚C, against an Ar counterflow, 3.00 mL (9.0 mmol) of a 3.0 M CH_3CH_2MgBr solution in Et_2O was added by syringe. The reaction mixture was stirred and slowly warmed to room temperature. After 2 h, a yellow solution and an off-white precipitate form. The reaction mixture was stirred for 16 h after which time the solvent was removed and replaced with 10 mL of petroleum ether. The product was extracted several times with petroleum ether followed by slow cooling to -78 ˚C to afford 0.205 g (15.3%) of an oily yellow solid identified as **4**.

Major isomer (**4a**) (95%) ^{1}H NMR -30 ˚C (toluene-d_8): δ = -2.60 (s, 1H, Nb-*H*); 0.16 (s, 3H, SiMe_2); 0.08 (s, 3H, SiMe_2); 0.85 (m, 2H, CH_2=CH_2, exo); 1.22 (d, 7 Hz, 3H, CHMe_2); 1.26 (d, 7 Hz, 3H, CHMe_2); 1.37 (m, 1H, CH_2=CH_2, endo); 1.48 (m, 1H, CH_2=CH_2, endo); 2.81 (sept, 7 Hz, 1H, C*H*Me_2); 3.18, 3.19, 4.24, 4.28, 5.24, 5.26, 5.80 (m, 1H, Cp). ^{13}C NMR (benzene-d_6): δ = -6.79 (SiMe_2); -4.19 (SiMe_2); 11.25 (*C*H_2=CH_2, endo); 20.54 (CH_2=CH_2, exo); 23.93 (CHMe_2); 24.52 (CHMe_2); 28.96 (*C*HMe_2); 70.56, 71.97, 82.94, 84.66, 91.71, 93.00, 103.30, 104.65, 106.23, 136.86 (Cp).

Minor isomer (**4b**) (5%) ^{1}H NMR -30 ˚C (toluene-d_8): δ = -2.69 (s, 1H, Nb-*H*); 0.13 (s, 3H, SiMe_2); *not located* (s, 3H, SiMe_2); 0.96 (m, 2H, CH_2=CH_2, exo); 1.57 (m, 2H, CH_2=CH_2, endo); *2 not located* (CHMe_2); 2.67 (m, 1H, C*H*Me_2); 3.43, 5.03 (2H), 5.53, 5.76, *2 not located* (m, 1H, Cp). ^{13}C NMR (benzene-d_6): δ = -6.53 (SiMe_2); -4.49 (SiMe_2); 12.88 (*C*H_2=CH_2, endo); 18.27 (CH_2=CH_2, exo); 21.58 (CHMe_2); 25.77 (CHMe_2); 31.72 (*C*HMe_2); 85.01, 85.22, 93.29, 100.13, 102.26, 105.70, *4 not located* (Cp).

[Me_2Si(η^5-C_5H_4)(η^5-C_5H_3-3-CMe_3)]Nb(η^2-CH_2CH_2)H (5). This compound was prepared in a manner similar to that for **4** employing 0.180 g (0.444 mmol) of **2**, 326 μL (0.98 mmol) of a 3.0 M CH_3CH_2MgBr solution in Et_2O, and Et_2O as the solvent. Extraction with petroleum ether followed by slow cooling to -40 ˚C afforded 0.044 g (27%) of a yellow crystalline solid identified as **5**. ^{1}H NMR (benzene-d_6): δ = -2.56 (s, 1H, Nb-*H*); 0.10 (s, 3H, SiMe_2); 0.19 (s, 3H, SiMe_2); 0.91

(m, 2H, CH_2=CH_2, exo); 1.33 (s, 9H, CMe_3); 1.42 (m, 2H, CH_2=CH_2, endo); 3.16, 3.19, 4.19, 4.25, 5.27 (2H), 5.86 (m, 1H, Cp). ^{13}C NMR (benzene-d_6): δ = -6.94 (SiMe_2); -4.04 (SiMe_2); 11.17 (CH_2=CH_2, endo); 21.51 (CH_2=CH_2, exo); 31.85 (CMe_3); 32.00 (CMe_3); 70.18, 71.62, 81.22, 83.97, 92.09, 93.60, 102.55, 103.58, 105.46, 142.81 (Cp).

[$Me_2Si(\eta^5$-C_5H_3-3-$CMe_3)_2$]Nb(η^2-CH_2CH_2)H (6ab). This compound was prepared in a manner similar to that for **4** employing 0.286 g (0.619 mmol) of **3**, 0.480 mL (1.4 mmol) of a 3.0 M CH_3CH_2MgBr solution in Et_2O, and Et_2O as the solvent. Extraction with petroleum ether followed by slow cooling to -40 ˚C afforded a yellow crystalline solid identified as the *meso* isomer **6a**. Subsequent fractional recrystallization allows separation of *rac* and *meso* isomers (0.030 g *meso* isomer **6a** isolated; 12% of total yield). The *rac* isomer (**6b**) is isolated as an orange oil.

meso Isomer (**6a**) (50%) ^{1}H NMR (500 MHz, toluene-d_8): δ = -2.70 (s, 1H, Nb-*H*); 0.15 (s, 3H, SiMe_2); 0.21 (s, 3H, SiMe_2); 0.87 (m, 2H, CH_2=CH_2, exo); 1.28 (s, 18H, CMe_3); 1.37 (m, 2H, CH_2=CH_2, endo); 3.16, 4.28, 5.26 (m, 2H, Cp). ^{13}C NMR (300 MHz, toluene-d_8): δ = -6.91 (SiMe_2); -3.73 (SiMe_2); 12.57 (CH_2=CH_2, endo); 22.60 (CH_2=CH_2, exo); 26.16 (CMe_3); 32.14 (CMe_3); 69.64, 81.19, 92.99, 102.13, 143.10 (Cp).

rac Isomer (**6b**) (50%) ^{1}H NMR (300 MHz, toluene-d_8): δ = -2.39 (s, 1H, Nb-*H*); 0.18 (s, 3H, SiMe_2); 0.25 (s, 3H, SiMe_2); *not located* (CH_2=CH_2, exo); 0.89 (s, 9H,

C*Me*$_3$); *not located* (C*H*$_2$=CH$_2$, endo); 1.29 (s, 9H, C*Me*$_3$); 3.15, 4.24, 4.27, 5.25, 5.34, 5.89 (m, 1H, Cp). ^{13}C NMR (500 MHz, toluene-*d*$_8$): δ = -6.84 (Si*Me*$_2$); -3.33 (Si*Me*$_2$); 11.10 (*C*H$_2$=CH$_2$, endo); 17.85 (CH$_2$=*C*H$_2$, exo); 30.60, 32.07 (C*Me*$_3$); *not located* (*C*Me$_3$); 69.97, 72.42, 81.38, 85.96, 91.70, 95.65, 102.06, 102.43, 130.65, 142.87 (Cp).

[Me$_2$Si(η^5-C$_5$H$_4$)(η^5-C$_5$H$_3$-3-CHMe$_2$)]Nb(η^2-CH$_2$CHPh)H (7abc). This compound was prepared in a manner similar to that for **4** employing 2.00 g (5.09 mmol) of **1**, 12 mL (12 mmol) of a 1.0 M PhCH$_2$CH$_2$MgCl solution in THF, and Et$_2$O as the solvent. Extraction with petroleum ether followed by removal of the solvent in vacuo afforded 0.325 g (15.0%) of an oily yellow solid identified as **7**.

Major isomer (**7a**) (53%) ^{1}H NMR (benzene-*d*$_6$): δ = -1.96 (s, 1H, Nb-*H*); -0.04 (s, 3H, Si*Me*$_2$); 0.08 (s, 3H, Si*Me*$_2$); 1.07 (dd, 10 Hz, 5 Hz, 1H, C*H*$_2$=CHPh, *trans*); 1.21 (d, 7 Hz, 3H, CH*Me*$_2$); 1.32 (d, 7 Hz, 3H, CH*Me*$_2$); 1.46 (dd, 13 Hz, 5 Hz, 1H, C*H*$_2$=CHPh, *cis*); 2.80 (sept, 7 Hz, 1H, C*H*Me$_2$); 3.50 (m, 1H, CH$_2$=C*H*Ph); 3.58, 3.60, 4.35, 4.38, 4.96, 5.14, 5.49 (m, 1H, Cp). ^{13}C NMR (benzene-*d*$_6$): δ = -6.04 (Si*Me*$_2$); -3.94 (Si*Me*$_2$); 19.96 (*C*H$_2$=CHPh); 24.77 (CH*Me*$_2$); 25.15 (CH*Me*$_2$); 29.67 (*C*HMe$_2$); 39.43 (CH$_2$=*C*HPh); 73.63, 75.06, 85.55, 88.63, 94.21, 96.06, 105.15, 108.73, 113.36, 136.53 (Cp); 122.49 (C$_6$H$_5$, *para*); *not located* (C$_6$H$_5$, *ortho*); 128.20 (C$_6$H$_5$, *meta*); 153.23 (C$_6$H$_5$, *ipso*).

Minor isomer (**7b**) (38%) ^{1}H NMR (benzene-d_6): δ = -2.15 (s, 1H, Nb-*H*); -0.02 (s, 3H, Si*Me*$_2$); 0.09 (s, 3H, Si*Me*$_2$); 0.74 (d, 7 Hz, 3H, CH*Me*$_2$); 1.12 (dd, 10 Hz, 5 Hz, 1H, C*H*$_2$=CHPh, *trans*); 1.23 (d, 7 Hz, 3H, CH*Me*$_2$); 1.36 (dd, 13 Hz, 5 Hz, 1H, C*H*$_2$=CHPh, cis); 1.52 (sept, 7 Hz, 1H, CH*Me*$_2$); 3.50 (m, 1H, CH$_2$=C*H*Ph); 3.42, 3.45, 4.27, 4.30, 5.19, 5.55, 5.95 (m, 1H, Cp). 13C NMR (benzene-d_6): δ = -6.24 (Si*Me*$_2$); -3.67 (Si*Me*$_2$); 20.63 (*C*H$_2$=CHPh); 22.53 (CH*Me*$_2$); 26.43 (CH*Me*$_2$); 26.79 (*C*HMe$_2$); 37.93 (CH$_2$=*C*HPh); 73.83, 75.04, 82.96, 86.81, 95.31, 96.15, 104.16, 110.15, 113.34, 138.34 (Cp); 122.15 (C$_6$H$_5$, *para*); 127.45 (C$_6$H$_5$, *ortho*); not located (C$_6$H$_5$, *meta*); 152.95 (C$_6$H$_5$, *ipso*).

Trace isomer (7c) (9%) 1H NMR (benzene-d6): δ = -2.09 (s, 1H, Nb-*H*); -0.05 (s, 3H, Si*Me*$_2$); 0.06 (s, 3H, Si*Me*$_2$); 0.38 (dd, 10 Hz, 5 Hz, 1H, C*H*$_2$=CHPh, *trans*); 0.94 (d, 7 Hz, 3H, CH*Me*$_2$); *not located* (CH*Me*$_2$); *not located* (C*H*$_2$=CHPh, *cis*); *not located* (*C*HMe$_2$); *not located* (CH$_2$=*C*HPh); 4.15, 4.46, 4.67, 4.76, 4.92, 5.21, 5.32 (m, 1H, Cp). ^{13}C NMR (benzene-d_6): δ = -5.40 (Si*Me*$_2$); -4.71 (Si*Me*$_2$); 18.77 (*C*H$_2$=CHPh); 23.32 (*C*HMe$_2$); 24.36 (CH*Me*$_2$); 27.03 (CH*Me*$_2$); 39.21 (CH$_2$=*C*HPh); 89.41, 90.51, 92.66, 95.20, 100.53, 105.09, 112.02, 137.66 (Cp); 122.34 (C$_6$H$_5$, *para*); *not located* (C$_6$H$_5$, *ortho*); *not located* (C$_6$H$_5$, *meta*); 154.24 (C$_6$H$_5$, *ipso*).

[Me$_2$Si(η^5-C$_5$H$_4$)(η^5-C$_5$H$_3$-3-CMe$_3$)]Nb(η^2-CH$_2$CHPh)H (8ab). This compound was prepared in a manner similar to that for **4** employing 0.205 g (0.506 mmol) **2**, 1.11 mL (1.1 mmol) of a 1.0 M PhCH$_2$CH$_2$MgCl solution in THF, and Et$_2$O as the solvent. Extraction with petroleum ether followed by cooling to -40 ˚C afforded

0.054 g (24%) of a crystalline yellow solid identified as **8**.

Major isomer (**8a**) (90%) ^{1}H NMR (toluene-d_8): δ = -2.07 (s, 1H, Nb-*H*); -0.01 (s, 3H, SiMe_2); 0.12 (s, 3H, SiMe_2); 0.99 (dd, 10 Hz, 5 Hz, 1H, CH_2=CHPh, *trans*); 1.34 (s, 9H, CMe_3); 1.42 (dd, 13 Hz, 5 Hz, 1H, CH_2=CHPh, *cis*); 3.53 (dd, 13 Hz, 10 Hz, 1H, CH_2=C*H*Ph); 3.25, 3.44, 4.13, 4.18, 5.16, 5.25, 5.49 (m, 1H, Cp). ^{13}C NMR (toluene-d_8): δ = -6.94 (SiMe_2); -4.13 (SiMe_2); 20.96 (*C*H_2=CHPh); 32.13 (*C*Me_3); 32.21 (CMe_3); 37.81 (CH_2=*C*HPh); 73.00, 73.94, 82.70, 86.73, 96.48, 94.62, 104.20, 104.62, 111.90, 143.06 (Cp); 121.97 (C_6H_5, *para*); 127.28 (C_6H_5, *ortho*); 127.53 (C_6H_5, *meta*); 153.23 (C_6H_5, *ipso*).

Minor isomer (**8b**) (10%) ^{1}H NMR (toluene-d_8): δ = -1.98 (s, 1H, Nb-*H*); 0.05 (s, 3H, SiMe_2); 0.15 (s, 3H, SiMe_2); 0.83 (s, 9H, CMe_3); *not located* (1H, CH_2=CHPh, *trans*); *not located* (1H, CH_2=CHPh, *cis*); 3.18 (dd, 13 Hz, 10 Hz, 1H, CH_2=C*H*Ph); 3.07, 3.41, 4.00, 4.07, 5.09, 5.55, 6.13 (m, 1H, Cp). ^{13}C NMR (toluene-d_8): δ = -7.09 (SiMe_2); -3.51 (SiMe_2); *not located* (*C*H_2=CHPh); *not located* (*C*Me_3); 32.83 (CMe_3); 35.29 (CH_2=*C*HPh); 83.45, 85.24, 96.00, 100.23, 103.88, 106.11, 107.25, 121.59; *2 not located* (Cp); *not located* (C_6H_5, *ortho*); *not located* (C_6H_5, *meta*); *not located* (C_6H_5, *para*); *not located* (C_6H_5, *ipso*).

Crystallography: Crystal data, intensity collection, and refinement details are presented in Table 1 for compounds **5** and **8a**.

Data Collection and Processing: Data for compounds **5** and **8a** were collected on a Bruker SMART 1000 area detector running SMART.[26] The diffractometer was equipped with a Crystal Logic CL24 low temperature device and all datasets were collected at low temperature. The diffractometer used graphite-monochromated MoKα radiation with λ = 0.71073 Å.

The crystals were mounted on glass fibers with Paratone-N oil. Data were collected as ω–scans at three to six values (depending on the sample) of φ. For all crystals, the detector was 5 cm (nominal) distant at a θ angle of -28 °. The data were processed with SAINT.[31]

Table 1. X-ray Experimental Data.

Compound	**5**	**8a**
formula	$C_{18}H_{27}NbSi$	$C_{24}H_{31}NbSi$
formula weight	364.40	440.49
crystal system	monoclinic	Triclinic
space group	P $2_1/c$ (# 14)	P $\bar{1}$ (# 2)
a, Å	9.2022(6)	10.3001(11)
b, Å	21.1677(14)	10.5568(11)
c, Å	9.2632(6)	11.2207(12)
α, °	90	74.243(2)
β, °	108.940(1)	84.333(2)
γ, °	90	66.971(2)
volume, Å^3	1706.68(19)	1080.6(2)
Z	4	2

P_{calc}, g/cm^3	1.418	1.354
μ, mm^{-1}	0.76	0.62
F_{000}	760	460
crystal shape	lozenge	Lozenge
crystal color	yellow	Yellow
crystal size, mm	0.10 x 0.26 x 0.26	0.14 x 0.20 x 0.31
T, K	98	98
type of diffractometer	SMART 1000 ccd	SMART 1000 ccd
θ range, $^\circ$	1.9, 28.5	1.9, 28.5
h,k,l limits	-12, 12; -28, 28; -12, 12	-13, 13; -13, 14; -14, 14
data measured	25466	22478
unique data	4105	5072
data, $F_O>4\sigma(F_O)$	3597	4407
parameters / restraints	289/0	359/0
R1[a],wR2[b]; all data	0.028, 0.048	0.037, 0.051
R1[a],wR2[b]; $F_O>4\sigma(F_O)$	0.023, 0.048	0.031, 0.050
GOF[c] on F^2	1.84	1.53
$\Delta\rho$max,min, e·Å^{-3}	0.51, -0.37	0.60, -0.43

All data were collected with graphite monochromated MoKα radiation (λ=0.71073 Å).

[a] $R1 = \Sigma \, | \, |F_o| - |F_c| \, | \, / \, \Sigma |F_o|$

[b] $wR2 = \{ \Sigma[w(F_o^2-F_c^2)^2] \, / \, \Sigma[w(F_o^2)^2] \}^{1/2}$

[c] $GOF = S = \{ \Sigma[w(F_o^2-F_c^2)^2] \, / \, (n-p) \}^{1/2}$

Structure Analysis and Refinement: SHELXTL v5.1[31] was used to solve, via direct methods or by the Patterson method, and to refine all structures using full-matrix least-squares. All non-hydrogen atoms were refined anisotropically. For **5**, there is one molecule in the asymmetric unit. All hydrogen atoms, including the hydride, were refined isotropically. For **8a**, there is one molecule in the asymmetric unit. All hydrogen atoms, including the hydride, were refined isotropically.[27]

References

(1) For recent reviews see: (a) Brintzinger, H. H.; Fischer, D.; Mülhaupt, R.; Reiger, B.; Waymouth, R. M. *Angew. Chem. Int. Ed. Engl.* **1995**, *34*, 1143-1170. (b) Bochmann, M. *J. Chem. Soc., Dalton Trans.* **1996**, 255-270.

(2) (a) Piers, W. E.; Bercaw, J. E. *J. Am. Chem. Soc.* **1990**, *112*, 9406-9407. (b) Krauledat, H.; Brintzinger, H. H. *Angew. Chem. Int. Ed. Engl.* **1990**, *102*, 1412-1413. (c) Grubbs, R. H.; Coates, G. W. *Acc. Chem. Res.* **1996**, *29*, 85-93.

(3) Jordan, R. F. *Adv. Organomet. Chem.* **1991**, *32*, 325-387.

(4) Guerra, G.; Cavallo, L.; Moscardi, G.; Vacetello, M.; Corradini, P. *J. Am. Chem. Soc.* **1994**, *116*, 2988-2995.

(5) Pino, P.; Cioni, P.; Wei, J. *J. Am. Chem. Soc.* **1987**, *109*, 6189-6191.

(6) Pino, P.; Galimberti, M. *J. Organomet. Chem.* **1989**, *370*, 1-7.

(7) Waymouth, R. M.; Pino, P. *J. Am. Chem. Soc.* **1990**, *112*, 4911-4914.

(8) Gilchrist, J. H.; Bercaw, J. E. *J. Am. Chem. Soc.* **1996**, *118*, 12021-12028.

(9) (a) Broene, R. D.; Buchwald, S. L. *J. Am. Chem. Soc.* **1993**, *115*, 12569-12570. (b) Troutman, M. V.; Appella, D. H.; Buchwald, S. L. *J. Am. Chem. Soc.* **1999**, *121*, 4916-4917.

(10) Herzog, T. A.; Zubris, D. L.; Bercaw, J. E. *J. Am. Chem. Soc.* **1996**, *118*, 11988-11989.

(11) Veghini, D.; Henling, L. M.; Burkhardt, T. J.; Bercaw, J. E. *J. Am. Chem. Soc.* **1999**, *121*, 564-573.

(12) (a) Mise, T.; Miya, S.; Yamazaki, H. *Chem. Lett.* **1989**, 1853-1856. (b) Zhong, A. H.; Bercaw, J. E. *unpublished results.*

(13) (a) Doherty, N. M.; Bercaw, J. E. *J. Am. Chem. Soc.* **1985**, *107*, 2670-2682. (b) Burger, B. J.; Santarsiero, B. D.; Trimmer, M. S.; Bercaw, J. E. *J. Am. Chem. Soc.* **1988**, *110*, 3134-3146. (c) Ackerman, L. J.; Green, M. L. H.; Green, J .C.; Bercaw, J. E., *Organometallics* **2003**, *22*, 188-194.

(14) (a) Bailey, N. J.; Cooper, J. A.; Gailus, H.; Green, M. L. H.; James, J. T.; Leech, M. A. *J. Chem. Soc. Dalton Trans.* **1997**, 3579-3584. (b) Bailey, N. J.; Green, M. L. H.; Leech, M. A.; Saunders, J. F.; Tidswell, H. M. *J. Organomet. Chem.* **1997**, *538*, 111-118. (c) Conway, S. L.; Doerrer, L. H.; Green, M. L. H.; Leech, M. A. *Organometallics* **2000**, *19*, 630-637.

(15) (a) Antiñolo, A.; Martinez-Ripoll, M.; Mugnier, Y.; Otero, A.; Prashar, S.; Rodríguez, A. M. *Organometallics* **1996**, *15*, 3241-3243. (b) García-Yebra, C.; Carrero, F.; López-Mardomingo, C.; Fajardo, M.; Rodríguez, A. M.; Antiñolo, A.; Otero, A.; Lucas, D.; Mugnier, Y. *Organometallics* **1999**, *18*, 1287-1298. (c) Antiñolo A.; López-Solera I.; Orive I.; Otero A.; Prashar S.; Rodríguez A. M.; Villaseñor E. *Organometallics* **2001**, *20*, 71-78.

(16) (a) Herrmann, W. A.; Baratta, W. *J. Organomet. Chem.* **1996**, *506*, 357-361. (b) Herrmann, W. A.; Baratta, W.; Herdtweck, E. *Agnew. Chem. Int. Ed. Engl.* **1996**, *35*, 1951-1953.

(17) Chernega, A. N.; Green, M. L. H.; Suárez, A. G. *Can. J. Chem.* **1995**, *73*, 1157-1163.

(18) Shin, J. H.; Parkin, G. *Chem. Comm.* **1999**, 887-888.

(19) The NOE difference experiment for **4** was performed at -30 ˚C in order to obtain sharp NMR resonances and reliable structural data.

(20) Guggenberger, L. J.; Meakin, P.; Tebbe, F. N. *J. Am. Chem. Soc.* **1974**, *96*, 5420-5427.

(21) The structure of the isomer comprising 10% of the mixture has not been established, and thus it could be one of the four proximal isomers or one of the two exo distal isomers.

(22) Chirik, P. J. Ph.D. Thesis, California Institute of Technology, 2000. Zubris, D. L. Ph.D. Thesis, California Institute of Technology, 2001.

(23) Burger, B. J.; Bercaw, J. E. In *Experimental Organometallic Chemistry*; Wayda, A. L.; Darensbourg, M. Y., Eds.; ACS Symposium Series 357; American Chemical Society: Washington, DC, 1987, Chapter 4.

(24) Marvich, R. H.; Brintzinger, H. H. *J. Am. Chem. Soc.* **1971**, *93*, 2046-2048.

(25) Herzog, T. A. Ph.D. Thesis, California Institute of Technology, 1997.

(26) Bruker (1999) SMART, SAINT, and SHELXTL. Bruker AXS Inc., Madison, Wisconsin, USA.

(27) Crystallographic data for the structures of **5** (CCDC 147070) and **8a** (CCDC 147250) have been deposited with the Cambridge Crystallographic Data Centre

as supplementary publications. These data can be obtained free of charge via http://www.ccdc.cam.ac.uk/conts/retrieving.html (or from the Cambridge Crystallographic Data Centre, 12 Union Road, Cambridge CB2 1EZ, UK; fax: +44 1223 336033; or deposit@ccdc.cam.ac.uk). Structure factors are available electronically: e-mail: xray@caltech.edu.

Chapter 2

Experimental and Theoretical Studies of Olefin Insertion for *ansa*-Niobocene and *ansa*-Tantalocene Ethylene Hydride Complexes

The text of this chapter was taken in part from the following manuscript co-authored with Professors Malcolm Green and Jenny Green of Oxford University:

Ackerman, L. J.; Green, M. L. H.; Green, J .C.; Bercaw, J. E., *Organometallics* **2003**, *22*, 188-194.

Abstract

Using dynamic NMR methods the rates of hydrogen exchange following intramolecular ethylene insertion into the metal–hydride bond have been measured for the following group 5 *ansa*-metallocene complexes: $[Me_2Si(\eta^5\text{-}C_5H_4)(\eta^5\text{-}C_5H_3\text{-}3\text{-}R)]Nb(CH_2CH_2)H$ (R = $CHMe_2$, CMe_3), *rac*- and *meso*-$[Me_2Si(\eta^5\text{-}C_5H_3\text{-}3\text{-}CMe_3)_2]Nb(CH_2CH_2)H$ and $[(1,2\text{-}SiMe_2)_2(\eta^5\text{-}C_5H\text{-}3,5\text{-}(CHMe_2)_2)(\eta^5\text{-}C_5H_2\text{-}4\text{-}CMe_3)]Ta(CH_2CH_2)H$. The singly bridged *ansa*-niobocenes exchange up to 3 orders of magnitude faster than unbridged complexes. However, the doubly bridged *ansa*-tantalocene complex exchanges at a rate comparable to that previously reported for $(\eta^5\text{-}C_5Me_5)_2Ta(CH_2CH_2)H$ and much slower than a singly bridged complex, $[Me_2Si(\eta^5\text{-}C_5Me_4)_2]Ta(CH_2CH_2)H$. These "*ansa*-effects" were investigated by DFT calculations on model complexes. The computed exchange pathway showed the presence of an agostic ethyl intermediate. The calculated barriers for hydrogen exchange of model unbridged, singly bridged, and doubly bridged niobocenes correlate with the experimental results.

Introduction

Olefin insertion into a metal–hydrogen bond and the microscopic reverse, β-hydrogen elimination, are elementary reactions in organometallic chemistry. These transformations are of considerable interest due to their fundamental importance, as well as for their widespread occurrence in synthetic and catalytic processes. Both reactions occur in transition-metal-catalyzed processes such as olefin polymerization, isomerization, and hydrogenation.[1] Mechanistic studies on the reversible insertion of alkenes into M–H bonds have been carried out for a series of group 5 olefin hydride complexes (Figure 1).[2] These complexes exist

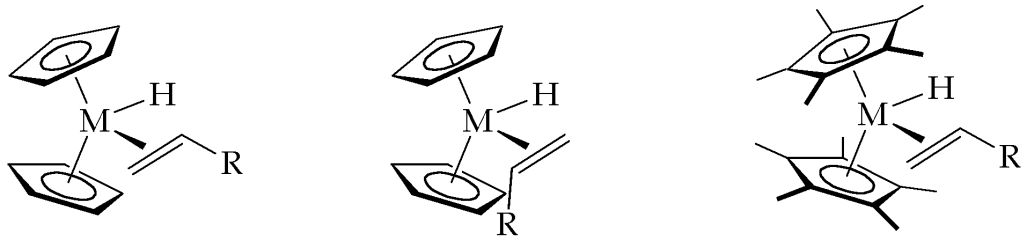

M = Nb; R = H, CH_3, Ph, C_6H_4-*m*-X, C_6H_4-*p*-X (X = CF_3, CH_3, OMe, NMe_2).
M = Ta; R = H, CH_3.

Figure 1. Group 5 olefin hydride complexes previously utilized to investigate olefin insertion into the M–H bond.

between two limiting resonance structures: d^2, M^{III} olefin hydride or d^0, M^V metallocyclopropane hydride (Scheme 1).

Rates of hydrogen exchange following olefin insertion were measured by either magnetization transfer or coalescence ^{1}H NMR techniques. The study revealed that the insertion step proceeds via a four-centered transition state with modest charge development:

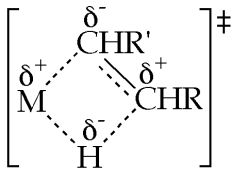

Thus, the transition state is stabilized when R is electron donating and R' is electron withdrawing. On the other hand, the ground-state olefin hydride complex is stabilized when both R and R' are electron withdrawing, due to stronger π-back-bonding interactions. The ground state is also stabilized for tantalum relative to niobium. This can be understood if the insertion process is

Scheme 1

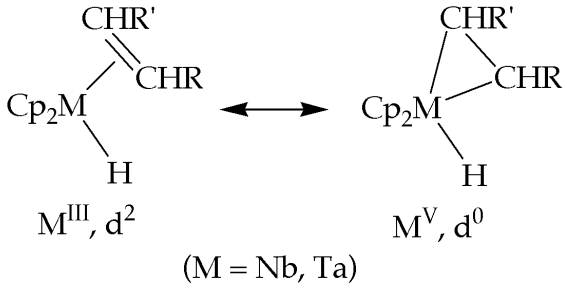

viewed as a reductive elimination of a C–H bond for the M^V, d^0 resonance structure, since higher oxidation states are generally preferred by the heavier congener of a periodic triad. Thus, the observed order of elimination rates is $k_{ins}(Nb) > k_{ins}(Ta)$.

When comparing the effect of ancillary ligands on the rate of insertion, one would expect the more electron-donating pentamethylcyclopentadienyl ligands (Cp*) to stabilize the M^V-like ground state relative to the M^{III}-like transition state. However, the Cp* ligands would have the opposite effect sterically, as they would destabilize the congested ground state relative to the

less crowded transition state. The activation barriers for representative complexes are summarized in Table 1. For the ethylene hydride complexes, $\Delta G^{\ddagger}$ (Cp*) > $\Delta G^{\ddagger}$ (Cp); thus, electronic effects dominate for the smallest olefin ligand. However, sterics dominate for larger olefins (propylene, styrene), since $\Delta G^{\ddagger}$ (Cp*) < $\Delta G^{\ddagger}$ (Cp).

Table 1. Activation Barriers for Olefin Insertion of Selected Complexes.[2]

Complex	$\Delta G^{\ddagger}$ (50 °C, kcal mol^{-1})
$Cp^*_2Nb(CH_2CH_2)H$	18.3(1)
$Cp_2Nb(CH_2CH_2)H$	17.1(1)
$Cp^*_2Nb(CH_2CHCH_3)H$	14.6(1)
$Cp_2Nb(CH_2CHCH_3)H$	16.5(1)
$Cp^*_2Nb(CH_2CHPh)H$	18.3(1)
$Cp_2Nb(CH_2CHPh)H$	20.5(1)

ansa-Metallocenes (Chart 1) have attracted much interest in Ziegler-Natta catalysis due to recent success in the development of stereospecific polymerization catalysts by strategic placement of substituents on the rigid *ansa*-metallocene fragment.[3,4,5] *ansa*-Metallocene complexes are also used as enantioselective catalysts for C–C and C–H bond formation.[6] More recently, doubly bridged *ansa*-metallocenes have been prepared and are among the most active catalysts for the syndiospecific polymerization of propylene (Chart 1).[7]

Chart 1

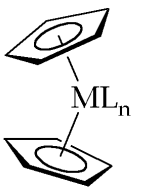

metallocene

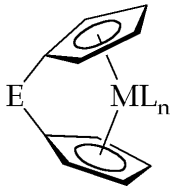

singly linked
ansa-metallocene

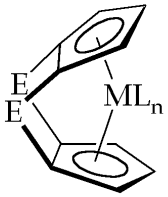

doubly linked
ansa-metallocene

(E = CH_2, CMe_2, CPh_2, $SiMe_2$, C_2H_4)

Thus, the investigation of ansa complexes in comparison with their nonbridged counterparts has been an active area of research.

Studies have revealed that in some cases the reactivity of an ansa complex is substantially different than that of an unbridged analogue. For example, the thermal stability of $[Me_2C(\eta^5\text{-}C_5H_4)_2]W(CH_3)H$ is much greater than that of $(\eta^5\text{-}C_5H_5)_2W(CH_3)H$.[8] The ansa complex is stable to reductive elimination of methane under thermal and photochemical conditions (up to 120 ˚C), but the unbridged complex loses methane at ca. 50 ˚C. A theoretical study by Jardine and Green revealed that after reductive elimination from the singlet methane σ complex, $\{(\eta^5\text{-}C_5H_5)_2W(CH_4)\}$, the proposed 16-electron intermediate, $\{(\eta^5\text{-}C_5H_5)_2W\}$, is able to relax to a low-energy, parallel ring triplet state, facilitating methane loss.[9] However, the ansa bridge constrains the rings, raising the triplet ground state of the intermediate such that little energy gain is possible upon methane loss. Other explanations have been proposed for the differing reactivity that the ansa bridge imparts in related metallocene systems. For example, Parkin has shown that the barrier to PMe_3 dissociation for

$[Me_2Si(\eta^5\text{-}C_5Me_4)_2]ZrH_2(PMe_3)$ is much larger than that for $Cp^*_2ZrH_2(PMe_3)$, with $k_{Cp^*} > 500k_{ansa}$ at 25 °C.[10] Shin and Parkin have also reported that the rate of olefin insertion for $[Me_2Si(C_5Me_4)_2]Ta(CH_2CH_2)H$ is 3 orders of magnitude faster than that for the corresponding unbridged complex, $Cp^*_2Ta(CH_2CH_2)H$.[11] These authors argue that the singly bridged ansa ligand is less electron donating than the unconstrained cyclopentadienyl ligands, resulting in a more electrophilic metal center. Hence, the zirconium center binds PMe_3 more tightly in the ansa complex. Similarly, the tantalum center back-bonds to the olefin π* orbital less efficiently for $[Me_2Si(C_5Me_4)_2]Ta(CH_2CH_2)H$; the ground state is destablized, and insertion is faster.

In this study, further investigations of ansa effects on olefin insertion have been undertaken by synthesizing and measuring hydrogen exchange rates for group 5 *ansa*-metallocene ethylene hydride compounds. Substitution patterns and the effects of introducing a second linking group for *ansa*-metallocene olefin hydride complexes have been investigated. DFT calculations have also been performed on model complexes.

Results and Discussion

Measurement of Hydrogen Exchange Rates. The *ansa*-niobocene and -tantalocene ethylene hydride complexes prepared for this study are shown in Chart 2. The synthesis and characterization (NMR, X-ray) of the complexes are reported elsewhere.[12] All complexes exhibit fluxional behavior observable by variable-temperature NMR due to olefin insertion into the M–H bond and

Chart 2

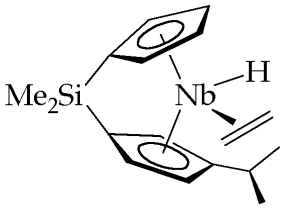

(1) iPrSpNb(CH_2CH_2)H

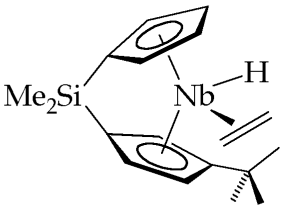

(2) tBuSpNb(CH_2CH_2)H

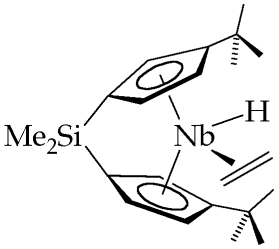

(3) *meso*-DpNb(CH_2CH_2)H

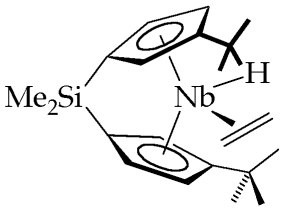

(4) *rac*-DpNb(CH_2CH_2)H

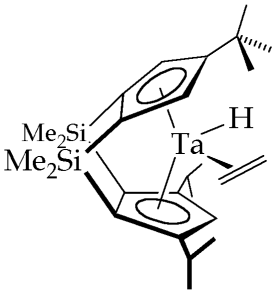

(5) tBuThpTa(CH_2CH_2)H

subsequent β-hydrogen elimination. Rates for this overall hydrogen exchange process upon ethylene insertion, C–C bond rotation for the ethyl product, and β-hydrogen elimination were determined by ^{1}H NMR line-shape analysis (all complexes) or magnetization transfer (complex **3**). The temperature-dependent broadening of the hydride resonance was used to calculate exchange rates in the line-shape simulations, assuming that the hydrogens become equivalent after insertion to form the ethyl complex. Magnetization transfer analysis was most

suitable for **3**, since the complex is C_s-symmetric, and the (equivalent) endo hydrogens undergoing exchange give rise to a well-defined triplet in the ^{1}H spectrum. On the other hand, analysis of magnetization transfer data for **1**, **2**, and **4** is complicated by the close proximity of the inequivalent endo hydrogens undergoing exchange and the complicated coupling patterns in these C_1-symmetric niobocenes.[13,14] Also, the endo and exo CH_2=CH_2 resonances are not well resolved for complex **5**. Nevertheless, the line-shape analysis data correlate well with magnetization transfer data for complex **3**, providing an independent check on the method (Figure 2).

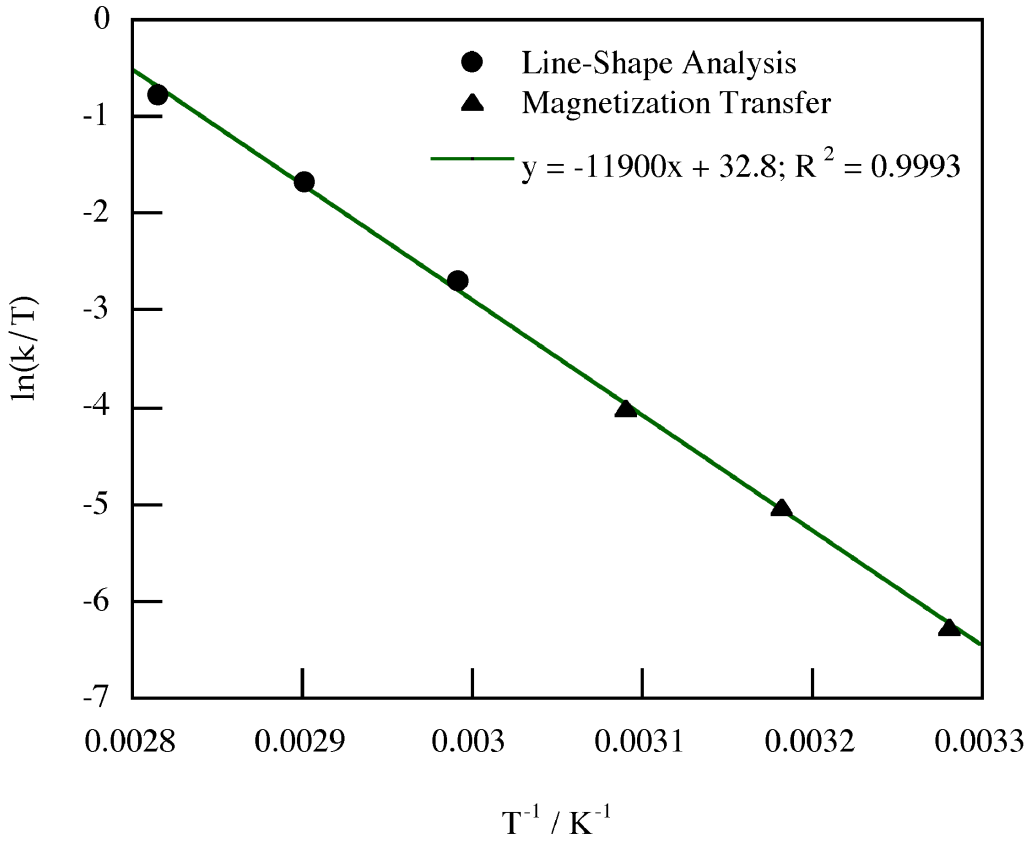

Figure 2. Eyring plot for endo methylene hydrogen/hydride exchange for complex **3** utilizing two different NMR methods: magnetization transfer and line-shape analysis.

Hydrogen exchange rate constants and free energies of activation at 318 K for *ansa*-niobocene complexes **1** - **4**, together with those for the previously studied complexes $(\eta^5\text{-}C_5H_5)_2Nb(CH_2CH_2)H$ and $(\eta^5\text{-}C_5Me_5)_2Nb(CH_2CH_2)H$ for

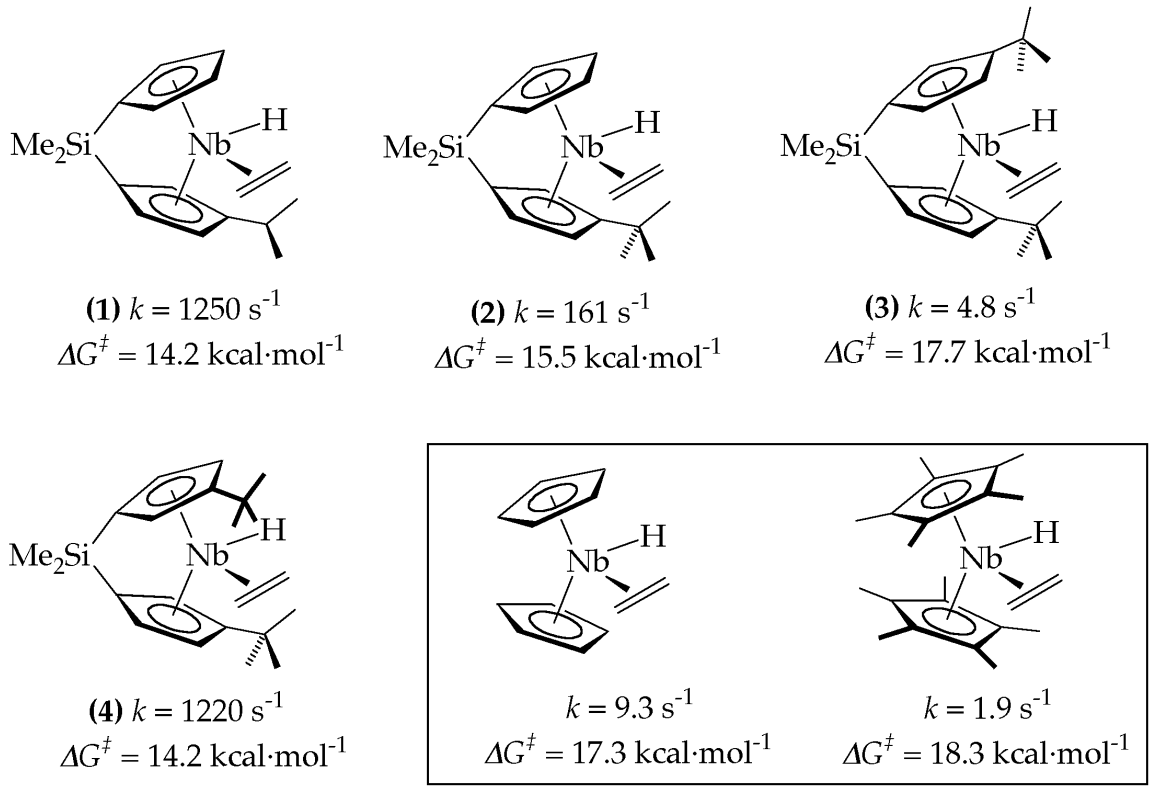

Figure 3. Olefin insertion rates and free energy barriers at 318 K for various niobocene ethylene hydride complexes. Rates for unbridged complexes (in box) have been reported in ref. 2.

comparison, are presented in Figure 3.[2] In agreement with Parkin's results for the *ansa*-tantalocene system (vide supra), the ansa ligand array appears to lower the activation barrier for hydrogen exchange compared to that for the unbridged complexes (complexes **1**, **2**, and **4**).[11] Although a direct comparison of $(\eta^5\text{-}C_5H_5)_2Nb(CH_2CH_2)H$ to $[Me_2Si(\eta^5\text{-}C_5H_4)_2]Nb(CH_2CH_2)H$ is lacking, there appear to be large ansa effects on the rates of hydrogen exchange, as evidenced

by the greater than 2 order rate increase for **1** vs $(\eta^5\text{-}C_5H_5)_2Nb(CH_2CH_2)H$. Less electron donation for a singly [$SiMe_2$]-bridged ligand relative to an unlinked analogue has been attributed to pulling of the cyclopentadienyl rings back toward η^3,η^3- hapticity.[10,11] More recently, infrared, electrochemical and DFT studies for a large number of zirconocene complexes have been undertaken to probe the effect of introducing single and double ansa linkages to the parent unlinked system.[15] These studies revealed lower electron density at the metal center for singly bridged metallocene fragments. By extension, the d^2 metal center of the $[Me_2Si(\eta^5\text{-}C_5H_4)_2]Nb(CH_2CH_2)H$ is expected to be less electron rich, and the ground state is electronically destabilized relative to $(\eta^5\text{-}C_5H_5)_2Nb(CH_2CH_2)H$.

That there are specific steric interactions influencing hydrogen exchange is evident from the decrease in rates going from **1** to **2**, but, most strikingly, by the large difference in exchange rates for **3** and **4**. The racemic complex, **4**, is among the fastest to undergo exchange, whereas the meso complex **3** exchanges on the same time scale as the unbridged complexes. This difference in rates for **3** and **4** can be attributed solely to steric placement of the *tert*-butyl groups, since the complexes are essentially identical electronically. Increasing the steric bulk from isopropyl (**1**) to one or two *tert*-butyl groups (**2**, **3**) on one side of the metallocene wedge successively decreases the rate of exchange, culminating with the drastically slower exchange rate observed for **3**. We postulate that the preference for ethylene to reside on the side of the niobocene wedge away from the isopropyl or *tert*-butyl group(s) is steric in origin and that the insertion transition structures that necessarily move the ethylene toward the hydride ligand on the

other side are increasingly crowded on going from **1** with one isopropyl substituent to **2** with one *tert*-butyl substituent to **3** with two *tert*-butyl substituents. The ethylene hydride complex **4** has more steric crowding than **1**, **2**, or **3**, since the *rac* isomer necessarily possesses a close *tert*-butyl/ethylene interaction. Thus, the ground state is destablized and the barrier for insertion is substantially reduced from that for **3**. Large steric effects have also been observed for the insertion of olefins into neutral group 4 zirconocene dihydrides.[16] The doubly [$SiMe_2$]-bridged *ansa*-tantalocene complex, **5**, was

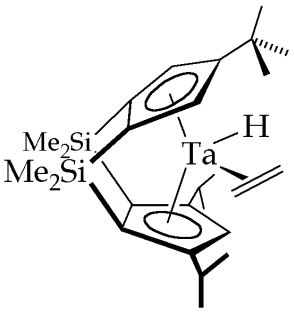

(5) $k = 24\ s^{-1}$

$\Delta G^{\ddagger} = 19.7\ kcal \cdot mol^{-1}$

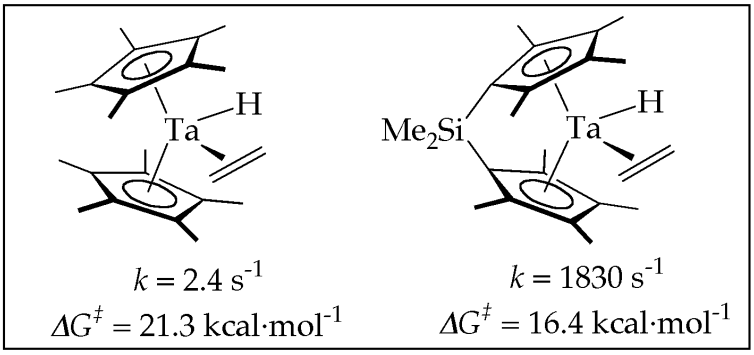

$k = 2.4\ s^{-1}$

$\Delta G^{\ddagger} = 21.3\ kcal \cdot mol^{-1}$

$k = 1830\ s^{-1}$

$\Delta G^{\ddagger} = 16.4\ kcal \cdot mol^{-1}$

Figure 4. Olefin insertion rates and free energy barriers at 373 K for various tantalocene ethylene hydride complexes. Rates for complexes (in box) have been reported in refs 2b and 11, respectively.

found to exchange at a rate more comparable to unlinked $(\eta^5\text{-}C_5Me_5)_2Ta(CH_2CH_2)H$ than to the singly [$SiMe_2$]-bridged *ansa*-tantalocene complex $[Me_2Si(\eta^5\text{-}C_5Me_4)_2]Ta(CH_2CH_2)H$ (Figure 4). At first sight it would appear puzzling that double linking of the cyclopentadienyl ligands has the net effect of unlinking them! Crystallographic data for $(\eta^5\text{-}C_5H_5)_2ZrCl_2$, $[Me_2Si(\eta^5\text{-}C_5H_4)_2\}ZrCl_2$, and $[(Me_2Si)_2(\eta^5\text{-}C_5H_3)_2]ZrCl_2$ show that the Cp_{cent}-Zr-Cp_{cent} angles decrease and the range of Zr–C bond lengths increases in a smooth progression as ansa linkages are introduced.[15a] With regard to the electronic effects of doubly linking the cyclopentadienyl ligands, these recent investigations indicated that the electron-donating effect of two vicinal [Me_2Si] ansa bridges in combination with a ligand conformation with an "η^2-ene-allyl" type coordination mode reduces back-donation from the metal to the cyclopentadienyl ligands.[15a] Hence, the d^2 metal center of $[(1,2\text{-}SiMe_2)_2(\eta^5\text{-}C_5H\text{-}3,5\text{-}(CHMe_2)_2)(\eta^5\text{-}C_5H_2\text{-}4\text{-}CMe_3)]Ta(CH_2CH_2)H$ is approximately as good a π donor, and the ground state is expected to be similar to $(\eta^5\text{-}C_5Me_5)_2Ta(CH_2CH_2)H$.

Density Functional Calculations. To increase understanding of the effect of single and double ansa bridges on the hydrogen exchange rate, density functional calculations were carried out on model systems, $[Cp^R{}_2Nb(C_2H_4)H]$, where $Cp^R{}_2$ = $(\eta^5\text{-}C_5H_5)_2$ (**6**), $[H_2Si(\eta^5\text{-}C_5H_4)_2]$ (**7**), and $(H_2Si)_2(\eta^5\text{-}C_5H_3)_2$ (**8**) (Chart 3). Four stationary points were identified on the hydrogen exchange surface for model complexes **6** - **8**: the ethylene hydride complex, $Cp^R{}_2Nb(\eta^2\text{-}C_2H_4)H$ = **a**, a β-agostic ethyl complex, $Cp^R{}_2Nb(\eta^2\text{-}C_2H_5)$ = **c**, an

Chart 3

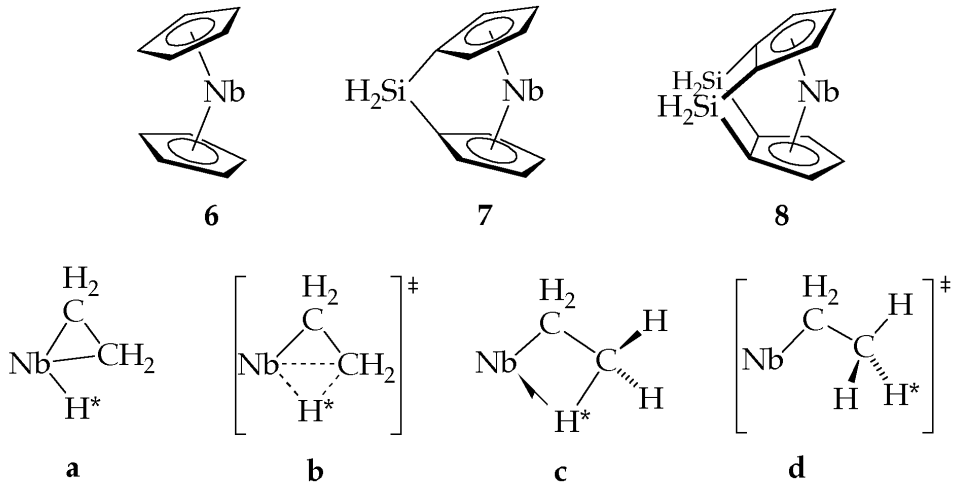

insertion transition state between these two minima, **b**, and the transition state for dissociation of the β-C–H bond, **d** (Chart 3).

Full geometry optimizations were carried out on all stationary points, and frequency calculations showed **a** and **c** to be local minima, having only positive frequencies, and **b** and **d** to be transition states, each having only one imaginary frequency. Energies relative to $Cp^R_2Nb(\eta^2\text{-}C_2H_4)H$ and key geometric parameters are given in Table 2.

Ground-State Structures. For all three ethylene hydride complexes, **6a** - **8a**, the Nb–H bond length is ca. 1.76 Å and the long C–C bond for the coordinated ethylene is around 1.43 Å. This latter value is in good agreement with the crystal structure of complex **2**, which has a C–C distance of 1.41 Å.[12] Such a bond length implies considerable back-donation to the olefin and an approach to a metallocyclopropane structure. The β-agostic ethyl structures, **c**, have very stretched agostic C–H bonds, ca. 1.2 Å, with the C–C bonds lengthened to around 1.50 Å. The Nb–H distances are consistent with agostic

bonding at 1.98-2.01 Å. With a 60˚ rotation about the C–C bond, the exchanging hydrogens become equivalent at the transition states **d**, which have normal ethyl groups with C–H bond lengths of 1.105-1.110 Å and C–C bond lengths ranging between 1.534 and 1.543 Å. The Nb–H contacts for **d** are now long, being greater than 2.6 Å. The greatest differences between the systems are calculated for the insertion transition states **b**, which, on distance criteria, appear to be earliest for **7** and latest for **8**. The relative cyclopentadienyl ring orientations are fixed for **7** and **8**, constrained by their respective bridges, and the variation in inter-ring angle is small as one follows the reaction progression from **a** to **d**. However, for **6** the rings are closer to being eclipsed than staggered. The unlinked **6a** and **6b** have a two-carbon front face conformation, as in **8**, but for **6c** and **6d**, the rings reorient to give a four-carbon front face conformation, as in **7** (Chart 4).[15a]

Chart 4

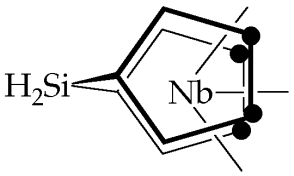

4-carbon front face

7

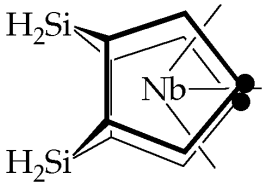

2-carbon front face

8

Mechanism for Hydrogen Exchange. Relative energies, given in Table 2 and represented diagrammatically in Scheme 2, concur well with the experimental values and trends, showing a significantly lower activation energy for the singly bridged system, **7**. The agostic ethyl, **c**, is lower in energy for **7** than for **6** or **8** (which fortuitously are calculated to have the same energy). As the insertion barrier and exchange barrier are also lower for **7**, this is consistent

with faster exchange rates measured for singly linked compounds. The energy differences between the agostic ethyl, **c**, and the transition state, **d**, are 2.0 kcal mol^{-1} for **6**, 1.9 kcal mol^{-1} for **7**, and 1.6 kcal mol^{-1} for **8**. Complex **8d** shows

Scheme 2

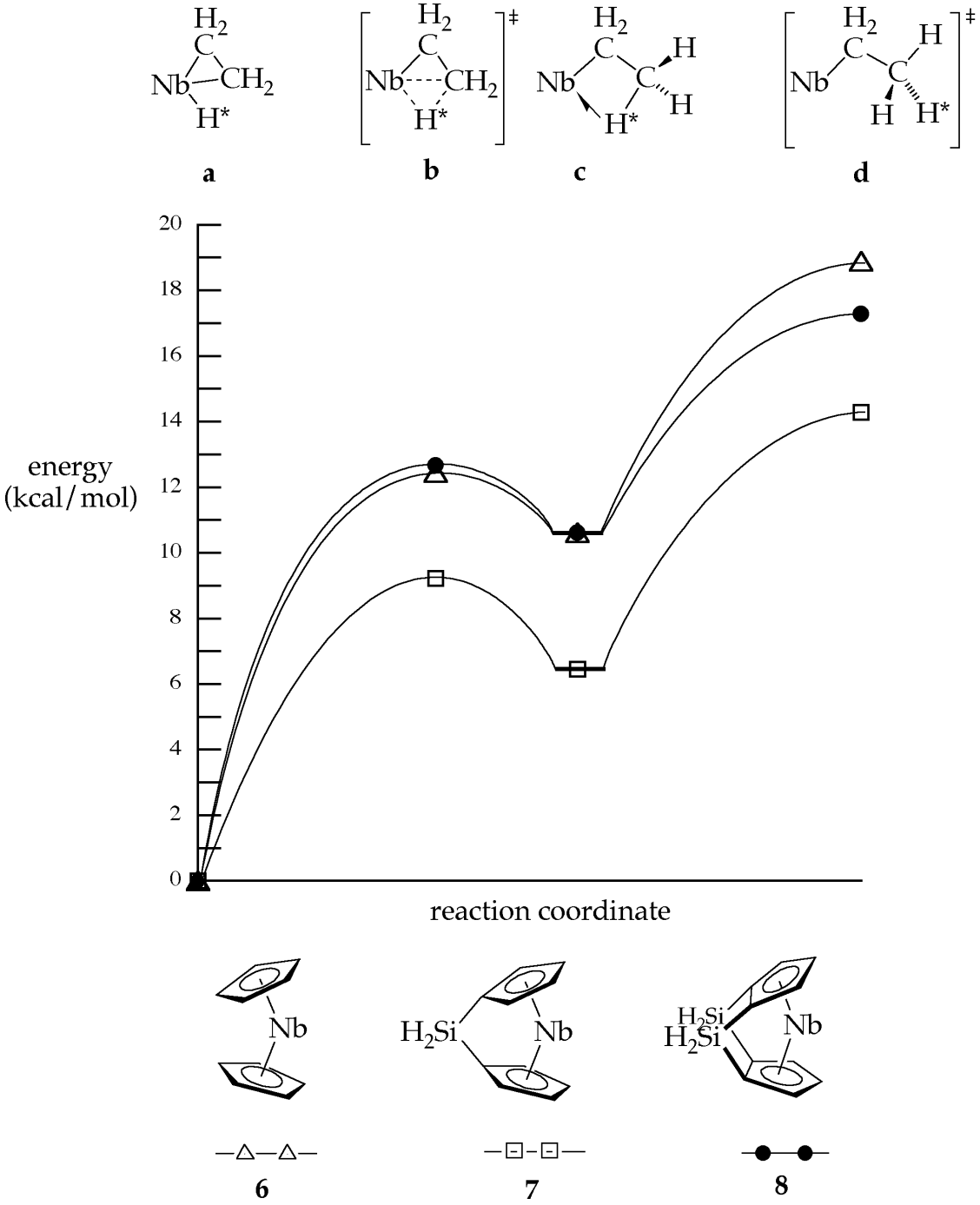

Table 2. Energies (kcal·mol^{-1}) and Selected Bond Lengths (Å) for **6** - **8**.

	Energy	Nb–H	C_{endo}–H	C–C	Nb–C_{exo}	Inter-ring Angle
6a	0	1.757	2.320	1.434	2.338	43
7a	0	1.765	2.332	1.427	2.344	54
8a	0	1.762	2.313	1.431	2.333	61
6b	12.45	1.814	1.430	1.466	2.299	38
7b	9.22	1.809	1.573	1.448	2.317	53
8b	12.68	1.881	1.385	1.478	2.281	58
6c	10.61	1.976	1.205	1.504	2.278	47
7c	6.46	1.988	1.200	1.503	2.268	53
8c	10.61	2.005	1.193	1.509	2.263	59
6d	18.91	2.856	1.105	1.543	2.265	48
7d	14.30	2.766	1.107	1.540	2.248	54
8d	17.30	2.681	1.110	1.534	2.249	60

marginally longer C–H bonds, and shorter Nb–H distances, suggesting that the transition state may maintain a very weak interaction between the exchanging hydrogens and the metal; however, for all three **d** is best described as a nonagostic ethyl. For all three systems a significant portion of the barrier to hydrogen exchange comes from the barrier to rotation of the methyl groups.

In previous studies of olefin insertion into group 5 metal–hydride bonds it has been assumed that, after the olefin inserts, there is a lower barrier to rotation about the C–C bond which exchanges the hydrogens, followed by fast

β-hydrogen elimination. An agostic interaction may or may not be cleaved following the insertion step to exchange the hydrogens (Scheme 3). The density functional calculations of this work support the formation and cleavage of a

Scheme 3

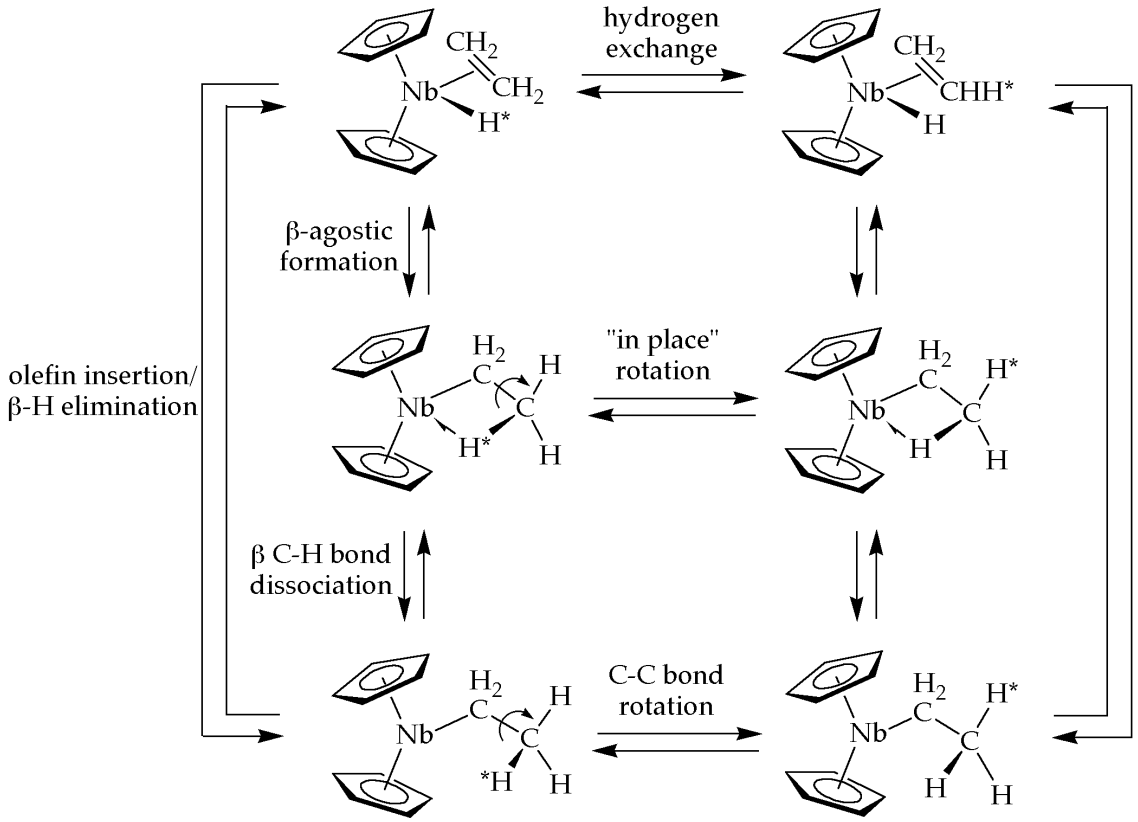

β-agostic structure to exchange the hydrogen atoms after the insertion event. Our research groups had earlier suggested that an "in-place" rotation mechanism will exchange hydrogen atoms after propene or ethylene insertion into a metal–hydride bond.[17] After insertion, the propyl or ethyl intermediate retains agostic bonding to the metal center while the hydrogens undergoing exchange rotate. Our calculations do not support this mechanism (except possibly for complex **8**; vide supra), but suggest that upon C–C bond rotation the agostic interaction is

completely broken. Hydrogen atom exchange can then be observed in the ^{1}H NMR spectrum following β-hydrogen elimination.

When the relative barriers for insertion versus hydrogen atom exchange were compared, it was unexpected that the highest free energy barrier along the reaction profile for hydrogen exchange was methyl rotation (Scheme 2). This conclusion raises questions concerning the interpretations of the steric and electronic effects for olefin insertion for this system, since previously the rate-determining step was assumed to be the insertion step.[2] On the other hand, the calculations reveal that the largest differences for **6** - **8** are the barriers for olefin insertion (**b**) and the energies for **c**. The barriers for methyl rotation (**d**) are quite similar for the three systems (with the caveat that the doubly [SiH_2]-bridged ansa complex has a slightly lower barrier, probably due to some weak agostic interactions as it rotates; vide supra). If this trend is general, i.e., the stereoelectronic influences on olefin insertion dominate, and the barriers for alkyl rotation are similar, then the principal conclusions reached from earlier studies are likely still valid.

Experimentally measuring these two separate barriers would be difficult for this group 5 metallocene system. Shultz and Brookhart have been able to measure independently the barriers to C–C bond rotation and β-H elimination for a cationic (diimine)Pd^{II} β-agostic ethyl complex by variable-temperature ^{1}H NMR.[18] For their palladium system the most stable structure is the β-agostic ethyl complex that exhibits three distinct resonances for the α- and β-methylene protons and the agostic proton at low temperatures. Upon warming, coalescence of the α-and β-methylene resonances is observed before the resonance for the

agostic β-proton displays any line broadening. Thus, the β-H elimination/olefin rotation/reinsertion process is faster than the C–C bond rotation process for the β-agostic ethyl ground state. Line shape analysis of the resonance for the β-agostic hydrogen at higher temperatures revealed the barrier to C–C bond rotation. At high temperatures, all five resonances coalesce as a result of the combination of the two processes. Thus, the barrier for β-H elimination, $\Delta G^{\ddagger}$(165 K), was established as 7.1 kcal·mol^{-1} and that for C–C bond rotation, $\Delta G^{\ddagger}$(165 K) as 8.4 kcal·mol^{-1}. For the group 5 metallocene ethylene hydride complexes the β-agostic ethyl is *not* the stable structure, and thus, a similar analysis is not possible.

Bonding Considerations. Formally, the formation of the ethyl transition state can be viewed as a reduction from Nb^{V} to Nb^{III}. Fragment analysis of the rotation transition states, **d**, confirm that these closely resemble a d^2 species where the two metal electrons occupy a d(x^2) metallocene orbital lying in the metallocene bonding plane. The stability of the analogous orbital in zirconocene compounds has been shown to vary in the order **7** > **6** > **8**;[15a] thus, the relative ease of exchange found here is entirely consistent with our previous study.

Conclusions

Rates of hydrogen exchange comprising olefin insertion, C–C bond rotation, and β-hydrogen elimination have been measured for a series of group 5 *ansa*-niobocene or -tantalocene ethylene hydride complexes. The data indicate that both the steric bulk and the placement of cyclopentadienyl substituents have

large effects on the energy barrier for hydrogen exchange. Exchange rates decrease by 3 orders of magnitude as the steric bulk is increased for those metallocenes with unsymmetrical substitution: the transition-state structure becomes more crowded as ethylene moves toward the hydride on the more sterically hindered side of the metallocene wedge. However, the ground-state structure can be destabilized by placing steric bulk on both sides of the metallocene wedge, resulting in a large enhancement in exchange rate. The exchange rate is 3 orders of magnitude larger for niobocenes with a single [$SiMe_2$] ansa bridge; however, little rate enhancement is observed for a complex with two [$SiMe_2$] bridges. The density functional calculations agree with this trend and suggest that the electron population shifts from the ground state to the transition state is the most favorable for the singly linked complex; hence, the fastest observed exchange rate.

Experimental

General Considerations. All air- and moisture-sensitive compounds were manipulated using standard vacuum line and Schlenk techniques or in a drybox under a nitrogen atmosphere as described previously.[19] Argon and dinitrogen gases were purified by passage over columns of MnO on vermiculite and activated molecular sieves. Toluene-d_8 was distilled from sodium benzophenone ketyl. NMR spectra were recorded on a Varian Inova or Unity$^+$ 500 MHz spectrometer (^{1}H, 500.13 MHz, ^{13}C, 125.77 MHz) or a Varian Mercury 300 MHz spectrometer (^{1}H, 300.07 MHz, ^{13}C, 75.45 MHz).

Magnetization Transfer Experiments and Line Shape Analysis

Experiments. For both types of experiments, the niobocene ethylene hydride samples were dissolved in toluene-d_8 and flame-sealed in NMR tubes under 700 Torr of argon at -78 ˚C. Reaction temperatures were determined by measuring the peak separation of an ethylene glycol or methanol standard before and after the experiments. For the line shape analysis, spectra were recorded in 10 degree increments for 40-50 degrees when the hydride resonance began to broaden. This broadening was simulated using gNMR.[20] Magnetization transfer spectra were obtained by using a DANTE pulse sequence.[21] Relaxation times (T_1) for the resonances of interest were measured at each temperature before the magnetization transfer experiment using the inversion recovery method. The magnetization transfer data were fitted using the program CIFIT to obtain rate constants.[22] The reported rate constants for the elementary chemical processes of insertion followed by C–C bond rotation, k, were calculated by multiplying the exchange rate constant (obtained by line shape analysis or magnetization transfer), k_{ex}, by a statistical factor (1.5) according to the following relationship:

$$k_{ex} = (2/3)k.$$

This statistical factor is necessary, because, on average, after insertion and C–C bond rotation, the same hydrogen returns to niobium or tantalum one-third of the time.

Computational Methods. Calculations were performed using density functional methods of the Amsterdam Density Functional Package (Versions ADF99.02 and ADF2000.02). The generalized gradient approximation method was employed, using the local density approximation of Vosko, Wilk, and

Nusair[23] together with non-local exchange corrections by Becke,[24] and non-local correlation corrections by Perdew.[25] Type IV basis sets used triple-ξ accuracy sets of Slater type orbitals, with a single polarization function added to main group atoms. The cores of the atoms were frozen up to 1s for C, 2p for Si and 3d for Nb. First order relativistic corrections were made to the cores of all atoms. Relativistic corrections were made using the ZORA (Zero Order Relativistic Approximation) formalism.

Reaction pathways were modeled by stepping a reaction coordinate through a sequence of fixed values and allowing the other structural parameters to optimize to a minimal energy.

All local minima and transition states were characterized by frequency calculations.

Fragment calculations were carried out to elucidate the trends in the electronic structure on an orbital basis. The fragments used were the $NbCp^R_2$ unit and the C_2H_4, H or C_2H_5 units with the identical geometry to that which they have in the optimized structure of the molecule.

References

(1) Parshall, G. W.; Ittel, S. D. *Homogeneous Catalysis 2nd Ed.* Wiley: New York, 1992; Ch 2-4.

(2) (a) Doherty, N. M.; Bercaw, J. E. *J. Am. Chem. Soc.* **1985**, *107*, 2670-2682. (b) Burger, B. J.; Santarsiero, B. D.; Trimmer, M. S.; Bercaw, J. E. *J. Am. Chem. Soc.* **1988**, *110*, 3134-3146.

(3) Brintzinger, H. H.; Fischer, D.; Müllhaupt, R.; Rieger, B.; Waymouth, R. M. *Angew. Chem. Int. Ed. Engl.* **1995**, *34*, 1143-1170.

(4) Kaminsky, W.; Kullper, K.; Brintzinger, H. H.; Wild, F. R. W. P. *Angew. Chem. Int. Ed. Engl.* **1985**, *24*, 507-508.

(5) Ewen, J. A.; Jones, R. L.; Razavi, A.; Ferrara, J. D. *J. Am. Chem. Soc.* **1988**, *110*, 6255-6256.

(6) Hoveyda, A. H.; Morken, J. P. *Angew. Chem. Int. Ed. Engl.* **1996**, *35*, 1262-1284.

(7) Herzog, T. A.; Zubris, D. L.; Bercaw J. E. *J. Am. Chem. Soc.* **1996**, *118*, 11988-11989.

(8) Labella, L.; Chernega, A.; Green, M. L. H. *J. Chem. Soc. Dalton Trans.* **1995**, 395-402.

(9) Jardine, C. N.; Green, J. C. *J. Chem. Soc. Dalton Trans.* **1998**, 1057-1061.

(10) Lee, H.; Desrosiers, P. J.; Guzei, I.; Rheingold, A. L.; Parkin, G. *J. Am. Chem. Soc.* **1998**, *120*, 3255-3256.

(11) Shin, J. H.; Parkin, G. *Chem. Comm.* **1999**, 887-888.

(12) Chirik, P. J.; Zubris, D. L.; Ackerman, L. J.; Henling, L. M.; Day, M. W.; Bercaw, J. E. *Organometallics* **2003**, *22*, 172-187.

(13) Magnetization transfer experiments were attempted for complex **1**, but the data could not be fitted within reasonable error limits.

(14) Typically, the magnetization transfer experiment is utilized to measure exchange between uncoupled protons (singlets in the ^{1}H spectrum). However, if the coupling is small compared to the chemical shift separation of the exchanging resonances (which is the case for **3**, but not for **1**, **2** and **4**), the magnetization transfer experiment can provide meaningful rate data.[2] For more details on this

subject see: Doherty, N. M. Ph.D. Thesis, California Institute of Technology, Appendix I, 1984 and references cited therein.

(15) (a) Zachmanoglou, C.; Docrat, A.; Bridgewater, B. M.; Parkin, G.; Brandow, C. G.; Bercaw, J. E.; Jardine, C. N.; Lyall, M.; Green, J. C.; Keister, J. *J. Am. Chem. Soc.* **2002**, *124*, 9525-9546. (b) Brandow, C. G. Ph.D. Thesis, California Institute of Technology, 2001. (c) Jardine, C. N. Ph.D. Thesis, St. Catherine's College, Oxford University, 2000.

(16) Chirik, P. J. Ph.D. Thesis, California Institute of Technology, 2000.

(17) (a) Green, M. L. H.; Sella, A.; Wong, L. *Organometallics* **1992**, *11*, 2650-2659.

(b) Derome, A. E.; Green, M. L. H.; Wong, L. *New J. Chem.* **1989**, *13*, 747-753.

(18) Shultz, L. H.; Brookhart, M. *Organometallics* **2001**, *20*, 3975-3982.

(19) Burger, B. J.; Bercaw, J. E. In *Experimental Organometallic Chemistry*; Wayda, A. L.; Darensbourg, M. Y., Eds.; ACS Symposium Series 357; American Chemical Society: Washington, DC, 1987, Chapter 4.

(20) Budzelaar, P. H. M. *gNMR for Macintosh, Version 3.6*; Cherwell Scientific Publishing Limited: Oxford, 1992-1996.

(21) Morris, G. A.; Freeman, R. *J. Magn. Reson.* **1978**, *29*, 433-462.

(22) Bain, A. D.; Cramer, J. A. *J. Magn. Reson.* **1996**, *118A*, 21-27.

(23) Vosko, S. H.; Wilk, L.; Nusair, M. *Can. J. Phys.* **1980**, *58*, 1200-1211.

(24) Becke, A. D. *Phys. Rev. Sect. A* **1988**, *38*, 3098-3100.

(25) (a) Perdew, J. P. *Phys. Rev. Sect. B* **1986**, *33*, 8822-8824. (b) Perdew, J. P. *Phys. Rev. Sect. B* **1986**, *34*, 7046.

Chapter 3

Arene C–H Bond Activation and Arene Oxidative Coupling by Cationic Palladium(II) Complexes

The text of this chapter was taken in part from the following manuscript:

Ackerman, L. J.; Sadighi, J. P.; Kurtz, D. M.; Labinger, J. A.; Bercaw, J. E. *Organometallics, submitted* **2003**.

Abstract

N,*N'*-Diaryl-α-diimine-ligated Pd(II) dimethyl complexes, ($^{tBu}{}_2{}^{Ar}$DAB^{Me})PdMe$_2$ and {$^{(CF_3)}{}_2{}^{Ar}$DAB^{Me}}PdMe$_2$ {$^{tBu}{}_2{}^{Ar}$DAB^{Me}: ArN=C(CH$_3$)–C(CH$_3$)=NAr, Ar = 3,5-di-*tert*-butylphenyl; $^{(CF_3)}{}_2{}^{Ar}$DAB^{Me}: Ar = 3,5-bis-(trifluoromethyl)phenyl} undergo protonolysis with HBF$_4$ (aq) in trifluoroethanol (TFE) to form cationic complexes [(α-diimine)Pd(CH$_3$)(H$_2$O)][BF$_4$]. The cations activate benzene C–H bonds at room temperature. Kinetic analyses reveal trends similar to those observed for the analogous Pt complexes: the C–H activation step is rate determining (KIE = 4.1 ± 0.5), and is inhibited by H$_2$O. The kinetic data is consistent with a mechanism in which benzene substitution proceeds by a solvent- (TFE-) assisted associative pathway. Following benzene C–H activation under 1 atm O$_2$, the products of the reaction are biphenyl and a dimeric μ-hydroxide complex, [(α-diimine)Pd(OH)]$_2$[BF$_4$]$_2$. The Pd(0) formed in the reaction is reoxidized by O$_2$ to the same dimeric μ-hydroxide complex after the oxidative C–C bond formation. The regioselectivity of arene coupling was investigated with toluene and α,α,α-trifluorotoluene as substrates.

Introduction

Selective hydrocarbon functionalization has been identified as an important challenge for academic and application-based chemical research.[1] Despite 30 years of research, a catalyst that displays the requisite activity, specificity, and durability has yet to be discovered. Our approach has been to focus on elucidating the mechanism of the Shilov system (Scheme 1), in which Pt(II) salts catalyze the oxidation of alkanes to alcohols (and alkyl chlorides) by Pt(IV) at 120 ˚C.[2] Studies by our group and others have elucidated a three-step catalytic cycle: (i) C–H bond activation, with liberation of a proton, to produce a Pt(II)-alkyl; (ii) oxidation of the Pt(II)-alkyl by $[PtCl_6]^{2-}$; and (iii) nucleophilic

Scheme 1

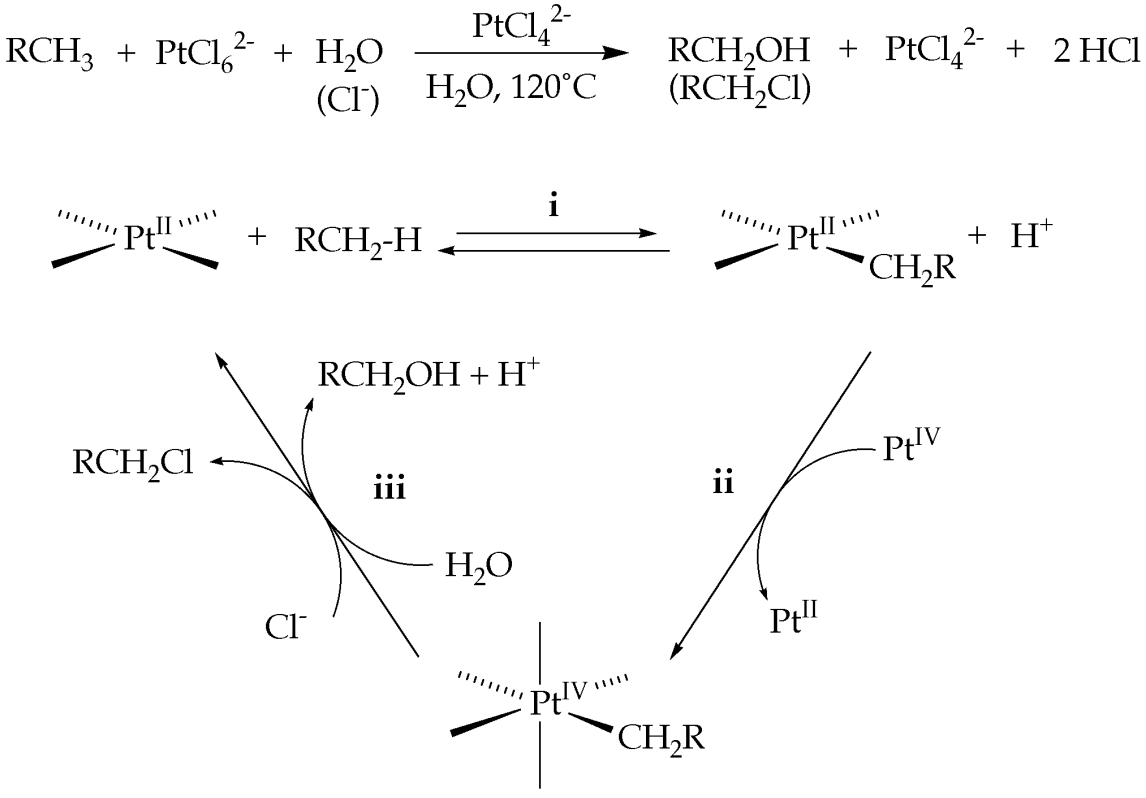

attack by water or chloride to liberate product and regenerate the Pt(II) catalyst.[3] Recent efforts in our group have focused on exploiting oxidation of Pt(II) complexes by O_2 (or other oxidants) to circumvent the use of stoichiometric Pt(IV).[4]

An alternate strategy for O_2 would employ a Pd(0)/Pd(II) redox couple to achieve the desired chemistry. Recently, oxidations of arenes to phenols[5] and of alcohols to aldehydes or ketones,[6] using Pd(II) catalysts and O_2 as the stoichiometric oxidant, have been reported. In addition, Stahl and coworkers demonstrated the clean reaction of [(bathocuproine)Pd(0)(η^2-dba)] (dba = dibenzylideneacetone) with O_2 to produce a Pd(II) peroxo complex, which liberates H_2O_2 upon treatment with acid (Scheme 2).[7] If Pd(II) complexes can effect C–H activation as well, then the catalytic cycle shown in Scheme 3 could be feasible.

Scheme 2

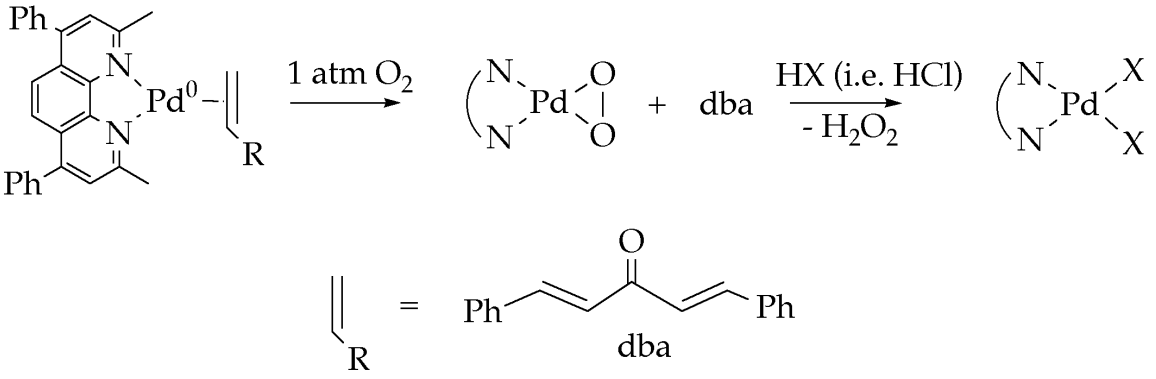

In Scheme 3, initial C–H bond activation, analogous to that observed in the Shilov system (**i**), is followed by a formal reductive elimination step (**ii**) to generate product and a Pd(0) fragment. Trapping and two-electron oxidation of

Scheme 3

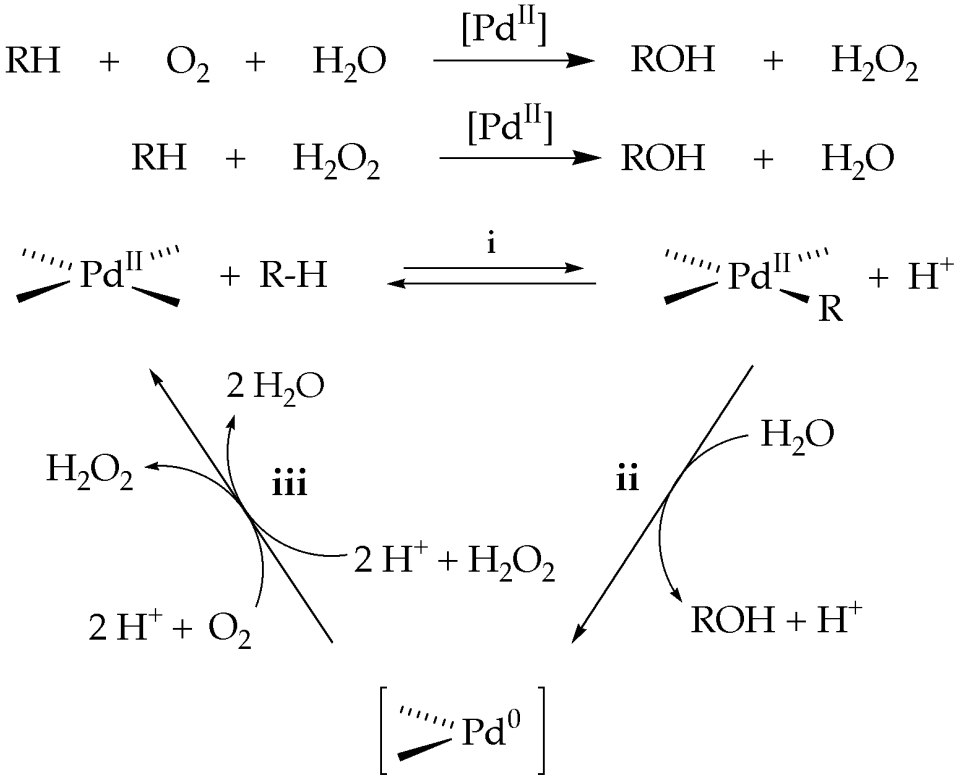

the product Pd(0) complex by O_2 would then regenerate the Pd(II) catalyst (step **iii**). The H_2O_2 byproduct of the oxidation could serve as another oxidizing equivalent, or it could disproportionate to H_2O and O_2 in the presence of Pd(II) as observed in other catalytic oxidation chemistry.[8] This proposed catalytic cycle is similar to that suggested by Periana and coworkers in the Hg(II)-catalyzed oxidation of methane to methyl bisulfate by H_2SO_4.[9] Since neither Hg(II) nor Pd(II) can easily access the (IV) oxidation state (in contrast to Pt), the proposed product release involves a reductive step, followed by reoxidation to the active catalyst species.

Mechanistic studies of C–H activation by [(α-diimine)Pt(CH_3)(H_2O)][BF_4] complexes such as **1a/b** have been reported.[10] Intramolecular C–H activation by similar cationic [(α-diimine)Pd(CH_3)(L)]$^+$ complexes has been observed.[11,12]

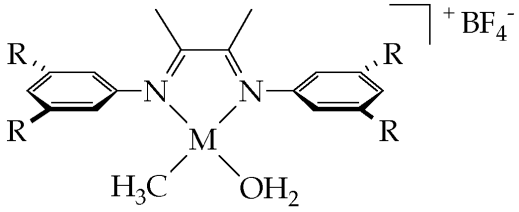

M = Pt
1a: R = CMe_3; **1b**: R = CF_3

M = Pd
2a: R = CMe_3; **2b**: R = CF_3

These results and the precedented reactivity of [(α-diimine)Pd(0)] complexes with O_2 (vide supra) directed us to investigate the intermolecular C–H activation of Pd(II) **2a** and **2b**.

Results and Discussion

Synthesis of Pd Complexes. The α-diimine ligands have been prepared previously by the formic acid-catalyzed condensation of 2,3-butanedione with the corresponding aniline in methanol.[10ab] Dimethyl Pd(II) complexes (α-diimine)$PdMe_2$, **3a** and **3b**, were prepared by treating [(pyridazine)$PdMe_2$]$_n$[13] and (COD)$PdMe_2$[14] (COD = 1,5-cyclooctadiene), respectively with the corresponding ligand.[11] Protonolysis of **3a/b** by HBF_4 (aq) in trifluoroethanol (TFE) solvent generates the methyl aquo cations, **2a/b**. The analogous reaction of Pt(II) dimethyl complexes affords an equilibrium mixture of aquo and

trifluoroethanol adducts observable by NMR; the magnitude of the equilibrium constant for different α-diimine complexes depends on the electron density at the Pt center, as assayed by CO stretching frequencies.[10a] Although we believe this aquo/solvento equilibrium is operative for **2a** or **2b** (vide infra), only one species is observed in the NMR spectra, even at low temperature or after addition of up to 50 μL of D_2O. Small chemical shift differences between the aquo and trifluoroethanol adducts of **2a/b**, and/or a low kinetic barrier for their interconversion may account for this observation. Complexes **2a/b** are prepared *in situ* and have not been isolated as analytically pure solids.

Kinetics of Reactions with Benzene. Methyl cations **2a/b** react with benzene in TFE-d_3, with concomitant liberation of methane. ^{1}H NMR was used to monitor the disappearance of starting material from which rates were determined. When carried out under an atmosphere of dioxygen, these reactions proceed cleanly, affording biphenyl and palladium(II) products (vide infra). On the other hand, when **2a/b** react with benzene under an inert atmosphere (e.g., Ar), palladium metal deposition accompanies biphenyl and soluble palladium(II) product formation. The rates are not affected by ionic strength: several experiments were conducted at different D_2O concentrations with and without added NMe_4BF_4 with negligible change in rate constants (see Appendix). Hence, kinetic studies were carried out under 1 atm O_2 without controlling ionic strength. As previously found for the analogous platinum systems,[10] the reaction is first-order in benzene, rates are decreased by added water, and $1/k_{obs}$ is linear with respect to $[D_2O]/[C_6H_6]$ (Figure 1).[15] Reactivity falls off in the order **2a** > **2b** > **1a**.

The temperature dependence for the reaction between **2a** and C_6H_6 was studied over the range of 1 – 40 ˚C. The activation parameters calculated from the Eyring plot are ($\Delta H^{\ddagger}$ = 20 ± 2 kcal·mol^{-1}, $\Delta S^{\ddagger}$ = -2 ± 6 e.u.) for C_6H_6 activation are similar to the values of $\Delta H^{\ddagger}$ = 20 kcal·mol^{-1}, $\Delta S^{\ddagger}$ = -5 e.u. for **1a**.[10a,16]

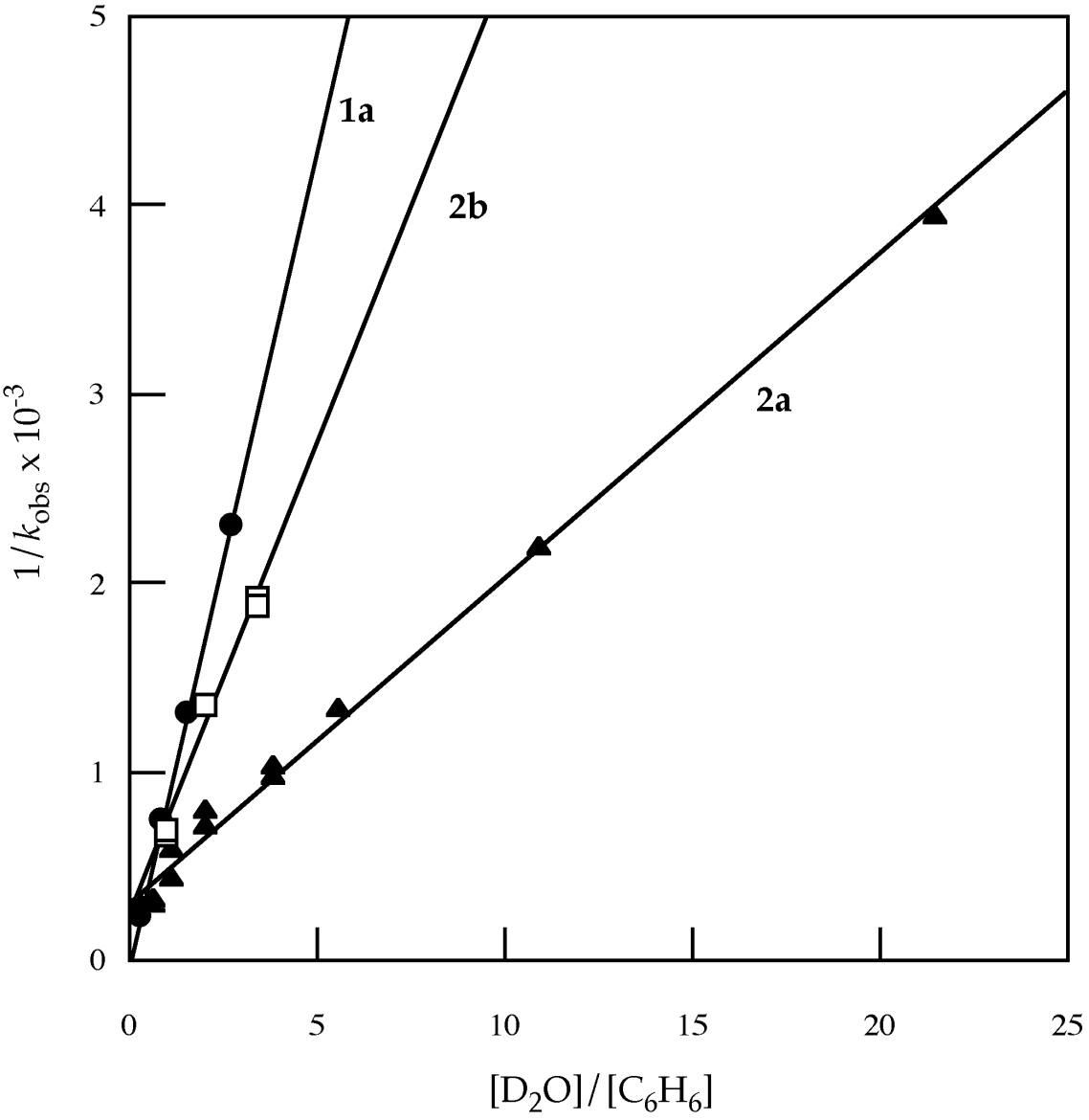

Figure 1. Plots of the reciprocal pseudo first order rate constants from the kinetics of reactions of [(α-diimine)M(CH_3)(H_2O)](BF_4) with C_6H_6 (298 K) at varying D_2O concentrations (M = Pd, Pt).

The kinetic isotope effect for the reaction was calculated by separately determining the rate constants for reactions of C_6H_6 and C_6D_6 under the same conditions. The measured isotope effect is 4.1 ± 0.5. The observed primary kinetic isotope effect indicates that C–H bond cleavage (k_2,Scheme 4) is rate-determining. Unlike **1a/b**, **2a/b** reacts with C_6D_6 to liberate only CH_3D without the observance of more highly deuterated methanes. Likewise, upon protonolysis of **3a/b** in TFE-d_3, only [(CH_3)Pd(II)] cations are formed, whereas the analogous Pt dimethyl complexes are converted to both [(CH_3)Pt(II)] and [(CH_2D)Pt(II)] cations.[10a] The exclusive formation of CH_3D in the deuterolysis of **3**, or in the reaction of **2** with deuterated benzene, indicates that the kinetic barrier to methane loss is small relative to that of the deuterium scrambling processes observed for **1a/b**. Deuterium scrambling for the Pt systems has been proposed to occur by formation of both methane and arene σ-complexes which undergo more than one oxidative addition/reductive elimination sequence before methane loss.[10ac]

Mechanism of C–H Activation of Benzene by Palladium(II) Methyl Cations. All of the observed data are consistent with the mechanism and derived rate law previously proposed for the analogous Pt systems (Scheme 4).[10ac]

In this scheme the aquo (**A*ii***) and solvento (**A*i***) complexes are in rapid equilibrium, with benzene displacing the more weakly bound solvent ligand; direct attack of benzene on **A*ii*** to displace water is assumed to be negligible. Rate determining C–H activation (k_2) occurs after benzene coordination (complex **B**). The accelerated rates observed for **2a** vs **2b** (ligand effects) and also **2a/b** vs

1a/b (metal effects) can be accounted for by the magnitude of K_{eq}. Although K_{eq} cannot be measured directly for **2a/b** (vide supra), it is calculated from the slope and intercept of the $1/k_{obs}$ plot (see Appendix for rate law derivation). The

Scheme 4

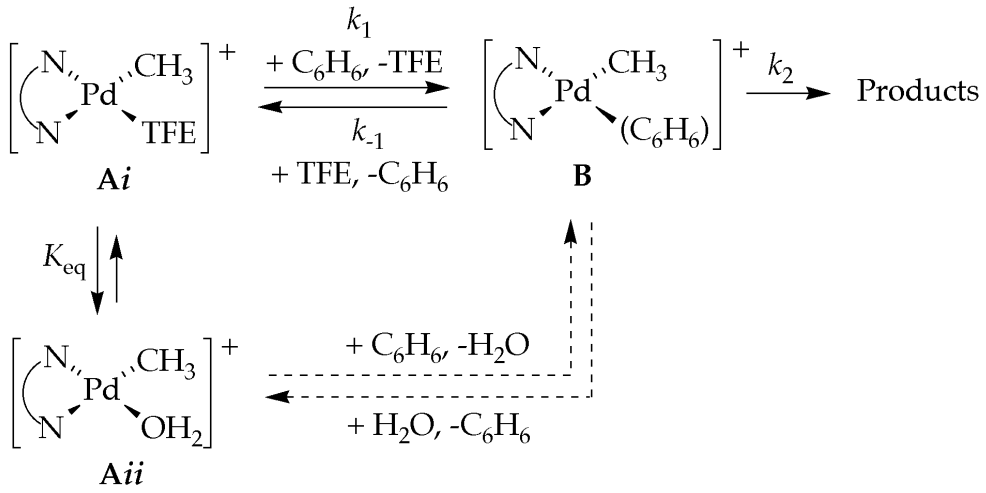

$$-\frac{d[\mathrm{Pd}]_T}{dt} = k_{obs}[\mathrm{Pd}]_T = \frac{k_2}{k_{-1}[\mathrm{TFE}] + k_2} \cdot \frac{k_1[\mathrm{TFE}][\mathrm{C_6H_6}][\mathrm{Pd}]_T}{[\mathrm{TFE}] + K_{eq}[\mathrm{H_2O}]}$$

calculated K_{eq} values for the palladium complexes are 36 for **2a** and 122 for **2b** (298 K). The measured K_{eq} values for the platinum congeners are 430 for **1a** and 2800 for **1b** (293 K).[10a] As reflected by the measured K_{eq} values, ground state differences between the aquo (**A*ii***) and solvento (**A*i***) complexes for a series of [(α-diimine)Pt(CH_3)(H_2O)][BF_4] complexes (including **1a/b**) were proposed to account for differences in C–H activation rate.[10a] The same behavior appears to be operative in the palladium cases. Thus, the more stable the aquo adduct (larger K_{eq}), the slower the C–H activation rate. The aquo adduct is more stable for the complexes with electron-withdrawing ligands (**1b** and **2b**) since the metal center is more electron-deficient, resulting in stronger bonding to the H_2O

molecule. In addition, the aquo adducts are more stable for the platinum complexes **1a/b** over the palladium analogs **2a/b** due to the stronger bonding of 5d transition metals to ligands compared to 4d transition metals.[17]

The kinetic data do not provide information about the exact nature of the C–H bond-breaking step for **2a/b** (e.g., oxidative addition vs σ-bond metathesis mechanisms). For platinum, a large body of evidence has been accumulated for a Pt(IV) hydride intermediate, supporting an oxidative addition mechanism for C–H activation by **1a/b**.[10ac,18] Because the Pd(IV) oxidation state is less readily accessible, the analogous intermediate may be less likely, although it cannot be ruled out. Canty and coworkers have structurally characterized a variety of Pd(IV) complexes, such as [(bipy)Pd(CH_3)$_3$I], obtained from oxidative addition of CH_3I to [(bipy)Pd(CH_3)$_2$].[19]

Reactivity of Palladium(II) Methyl Cations. Unlike their platinum congeners, **2a/b** do not form stable phenyl complexes upon reaction with benzene. As noted above, under an inert atmosphere reactions of **2a/b** with benzene deposit Pd(0) and produce unidentified palladium-containing byproducts and biphenyl. However, when the reaction is carried out under 1 atm of O_2, two identifiable Pd(II) species, [(α-diimine)Pd(H_2O)$_2$][BF_4]$_2$ (**4a/b**) and [(α-diimine)Pd(OH)]$_2$[BF_4]$_2$ (**5a/b**), as well as biphenyl form as the reaction proceeds. After complete reaction under O_2, the only products observed are **5a/b** and 0.5 equiv biphenyl, with no Pd(0) deposition.[20,21]

Complexes **4a** and **5a** were identified by independent syntheses from the dichloride ($^{tBu}{}_2{}^{Ar}$DAB^{Me})$PdCl_2$ (**6a**)[22,23] and isolation of the final product, **5a**, from the C–H activation reactions. **4a** and **5a** are synthesized by adding $AgBF_4$

to a solution of **6a** in wet CH_2Cl_2/THF (10/1) as published previously.[23] Notably, **4a** could be isolated as the sole product after the reported 3 h reaction time, but at shorter reaction times (1-2 h) mixtures of both **4a**, **5a**, and other unidentified species were observed. Dissolving the mixture in TFE-d_3 , followed by addition of HBF_4 (aq), results in the disappearance of the unidentified species, and only **4a** and **5a** are present in solution. Subsequent addition of HBF_4 converts all of **5a** to **4a**. **5a** is the sole product of the reaction of **2a** with benzene under O_2; the diagnostic protons on the bridging hydroxide groups were located in the ^1H NMR by evaporating the trifluoroethanol (protio solvent) and dissolving the residue in CD_2Cl_2. These protons on the bridging hydroxide groups appear at - 3.5 ppm and disappear upon addition of D_2O. In other dinuclear (diimine)Pd(II) hydroxide complexes, these hydrogens resonate near -3 ppm (CD_2Cl_2).[23]

The other species observed in the mixtures of **4a** and **5a** were not identified, but are most likely related complexes. Studies of the reaction of NaOH with N-ligated $[(L_2)Pd(OH)]_2[NO_3]_2$ complexes (L_2 = bipyridine or phenanthroline) in water have shown that several species form in solution which cannot be isolated in pure form.[24] The authors postulate that a trihydroxide bridged species may be a component of the mixture (Scheme 5).[24] Also, phosphine-ligated $[(BINAP)Pd(H_2O)_2][X]_2$ complexes have been isolated from the addition of AgX to the corresponding dichloride complexes (X = BF_4^- or OTf). Unlike **4a**, the dimers $[(BINAP)Pd(OH)]_2[X]_2$ are easily obtained from the bis(aquo) complexes by treating with 4 Å molecular sieves in acetone or treatment with 1 equiv NaOH. When an insufficient amount of sieves was used,

Scheme 5

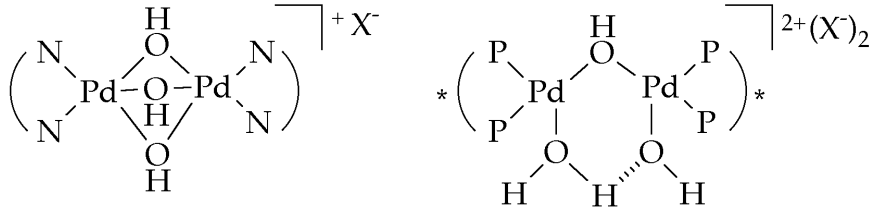

N-N = bipy, phen
$X = NO_3^-$

P-P* = tolyl-BINAP
$X = OTf^-$

a complex was isolated that was determined to be a binuclear mono-μ-hydroxo complex also having a (μ-HO···H···OH) as well (Scheme 5, ^1H NMR, ESI-MS).[25] These types of structures shown in Scheme 5 are likely related to the unidentified species observed for the α-diimine complexes in this study.

Although a hydroxide dimer complex could not be synthesized cleanly without some bis aquo complex, X-ray quality crystals of the hydroxide dimer complex **5b** were grown from an NMR tube reaction of **2b** and benzene (Figure 2). Details of the structure determination and labeled drawing are included in the Appendix.

Scheme 6 illustrates the proposed reaction sequence. The species, ***i***, ***ii***, and ***iii*** are unobserved, postulated intermediates. First, the phenyl product, ***i***, disproportionates (possibly by phenyl group transfer), to produce ***ii*** and **4a/b**. Reductive elimination of biphenyl from ***ii*** produces a Pd(0) complex, which is reoxidized by O_2 to peroxo intermediate ***iii*** or possibly by hydrogen peroxide to ***iii***.[7] Alternatively, hydrogen peroxide may be disproportionated rapidly.[8] Species similar to the postulated intermediates ***i*** and ***ii*** have been suggested for

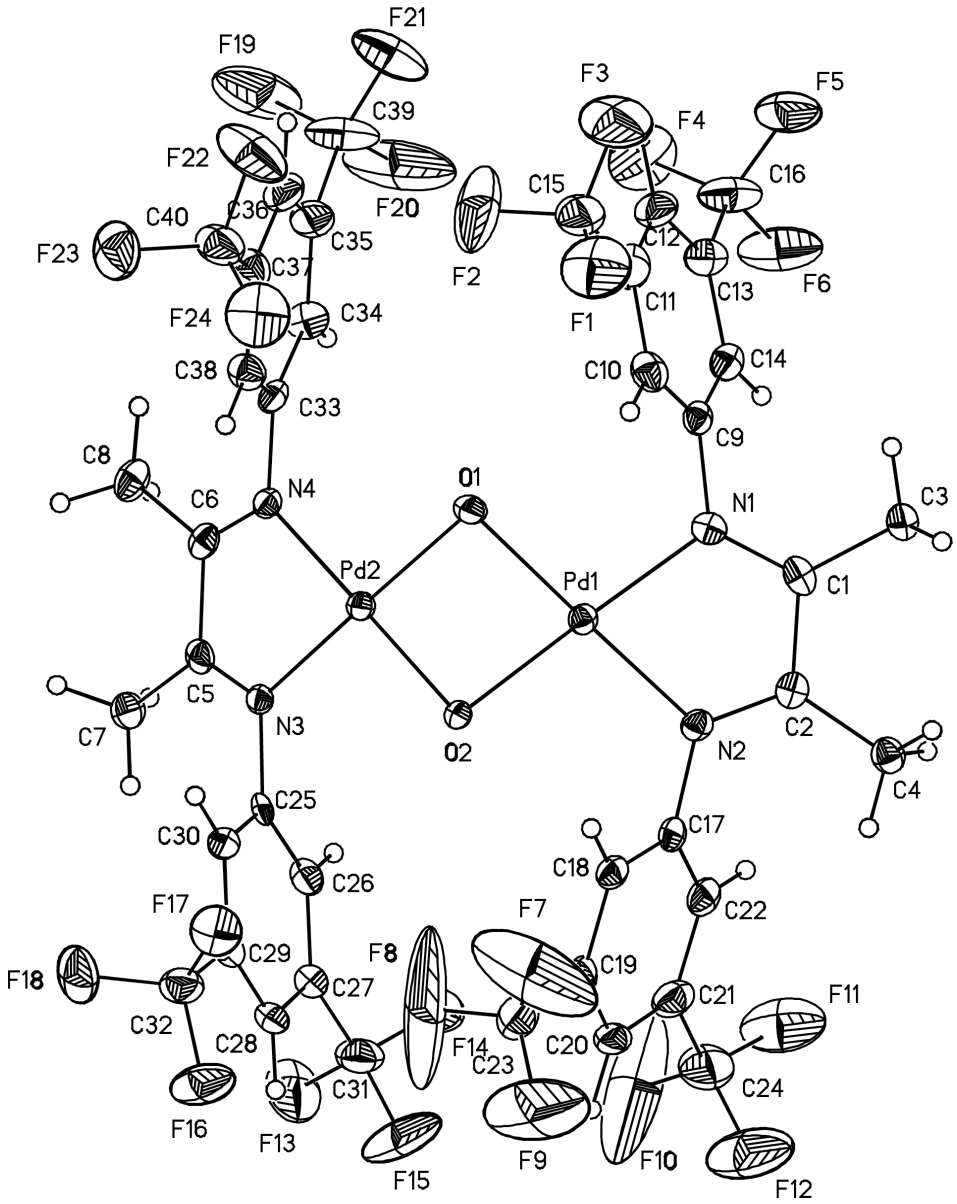

Figure 2. Molecular structure of **5b** with 50% probability ellipsoids. Hydrogen atoms and anions have been omitted. Selected bond distances (Å) and angles (deg) are as follows: Pd1–Pd2 = 2.9706, Pd1–N1 = 1.993(3), Pd1–N2 = 2.000(3), Pd1–O1 = 2.025(3), Pd1–O2 = 2.022(3), Pd2–N3 = 1.987(3), Pd2–N4 = 1.991(3), Pd2–O1 = 2.022(3), Pd2–O2 = 2.025(2), N1–Pd1–N2 = 79.03(13), N1–Pd1–O2 = 177.05(12), N1–Pd1–O1 = 99.60(12), Pd1–O1–Pd2 = 94.44(11), Pd1–O2–Pd2 = 94.45(11).

Scheme 6

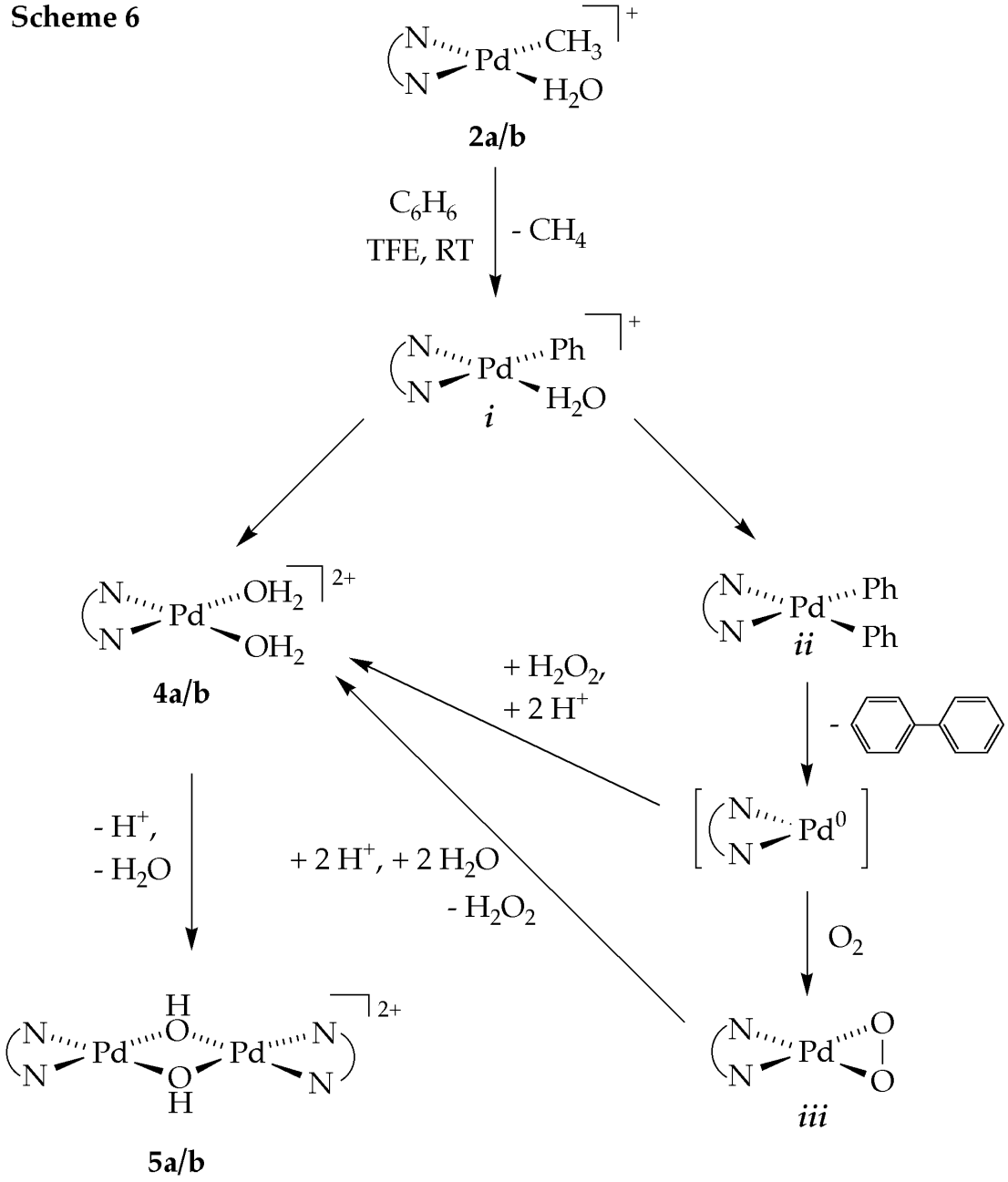

the intermolecular coupling of aryl ligands for $[(L_2)Pd(Ar)(solvent)][BF_4]$ (L_2 = N,N,N',N'-tetramethylenediamine, 2,2'-bipyridine, 4,4'-dimethyl-2,2'-bipyridine; solvent = THF, acetone, acetonitrile) and other related complexes.[26]

Other potential intermediates on the pathway to arene C–C coupling have been reported for similar Pt(II) systems. Recently, Kubas[27] and Peters[28] have isolated chelating bis(phosphine)Pt(II) dimer complexes which have a biphenyl unit sandwiched between the metal centers. One phenyl group of the biphenyl unit is bound as an η^3,η^3-bis-allyl to the two Pt centers, while the other remains aromatic. These unusual dimers were isolated after cationic or neutral Pt(II) phosphine complexes reacted with either benzene or toluene via C–H activation and subsequent C–C bond formation (eq 1). In the Kubas system, the formally

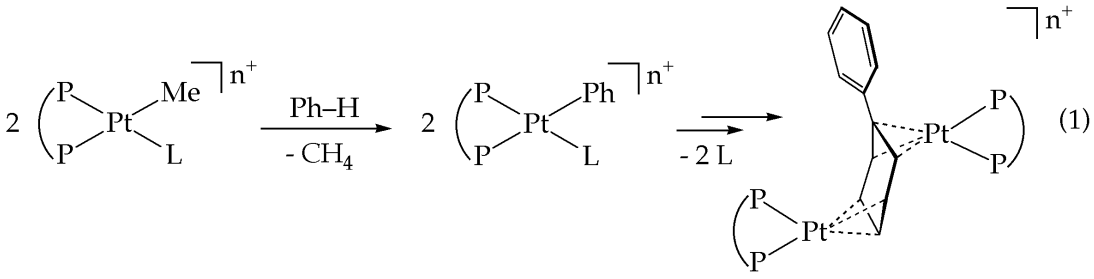

(1)

reduced biphenyl unit can be released upon oxidation with HCl to produce Pt(II) chloride dimers and H_2. These results led the authors to suggest that there is no formal redox reaction at Pt, and these dimers may resemble intermediates in Pd-mediated aryl coupling reactions. If such bis-allyl dimers are intermediates in this work, Pd acts as the oxidant for biphenyl release, since we observe Pd(0) deposition and the production of biphenyl (GC-MS) in the absence of oxidant.

Regioselectivity of Arene Coupling. Toluene and α,α,α-trifluorotoluene were investigated as substrates for arene coupling. Both substrates react with **2a** to produce mixtures of isomers as summarized in Scheme 7. Unfortunately, no substrate afforded a single coupled product which would be a synthetically useful feature of this reaction. Bitolyl products which are not commercially

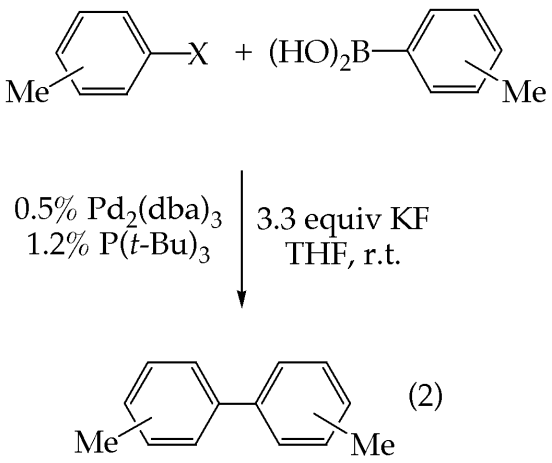

(2)

available were synthesized by the Suzuki coupling methodology developed by Fu (eq 2).[29] Bis(trifluoromethyl)biphenyl products were synthesized by oxidation of the aryl Grignard reagent by $TiCl_4$ (eq 3).[30] Toluene reacts with **2a**

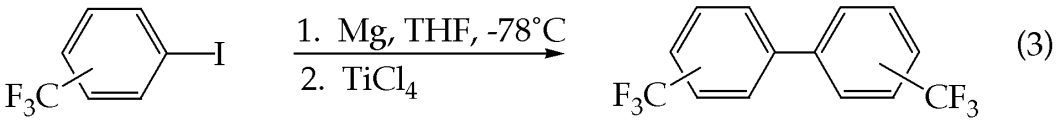

(3)

faster and trifluorotoluene slower than benzene by a factor of two and ten, respectively. The *o*:*m*:*p* regioselectivity is approximately 1:10:7 for toluene and 0:4:5 for trifluorotoluene (after statistical correction for the number of C–H bonds).

It is possible that the regioselectivity is determined during the reductive coupling from the postulated diphenyl palladium(II) intermediate, during transmetallation (Scheme 6), or during formation of a binuclear intermediate such as Kubas' $[L_4Pt_2(\mu_2\text{-}\eta^3,\eta^3\text{-}C_6H_5\text{-}Ph)]^{2+}$ (eq 1), if a different mechanism for C–C bond formation is occurring. On the other hand, if one assumes that the regioselectivity is determined by the C–H activation step, one may reconcile the observed regioselectivity as arising from a combination of steric and inductive

Scheme 7

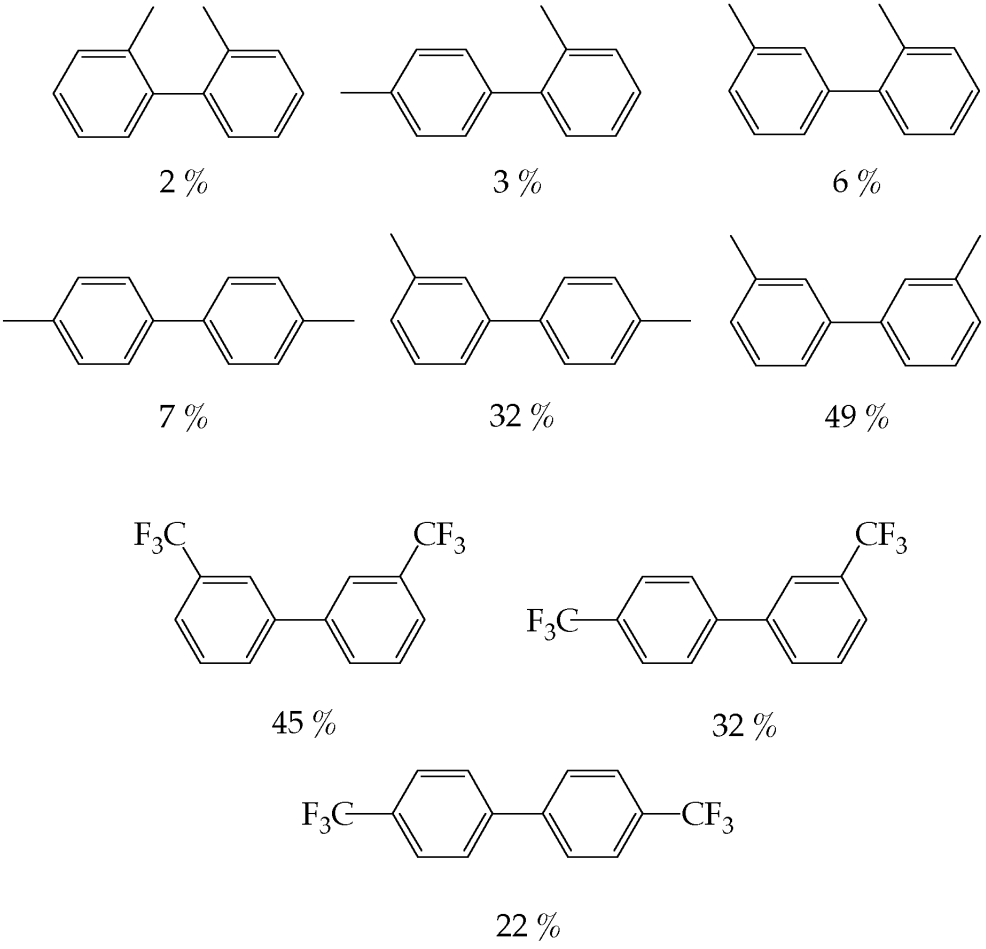

effects of the [CH_3] and [CF_3] substituents. Thus, the palladium center more readily activates the *meta* C–H positions over the *para* C–H position, since it is the more electron-rich site inductively; the *ortho* C–H positions are sterically hindered. Similarly, for trifluorotoluene, the *para* C–H position is more reactive because it is farthest from the strongly electron withdrawing [CF_3] group and thus most electron-rich, whereas the *ortho* C–H positions are most sterically hindered and least electron-rich. In agreement with this proposal that inductive electronic effects operate during the C–H bond activation step of these oxidative

coupling reactions of arenes, the second order rate constant for reaction **2a** with toluene (0.0124 M^{-1} s^{-1}) is significantly greater than that with α,α,α-trifluorotoluene (0.0005 M^{-1} s^{-1}).

Conclusions

Stoichiometric C–H bond activation of benzene by cationic Pd(II)-methyl complexes has been observed under mild conditions. Kinetic studies of the C–H activation step for the palladium complexes reveal that the C–H activation step is rate-determining and inhibited by H_2O. The data suggest that coordinated H_2O must be displaced by solvent (trifluoroethanol) before benzene coordination and subsequent C–H activation. The rates of C–H activation are increased by destabilizing the ground state aquo complex with relatively electron-donating ancillary ligands. Also, the ground state aquo complexes are destabilized for Pd relative to Pt, resulting in faster C–H activation rates. Finally, the barrier to methane loss for Pd is small, and in contrast with the analogous Pt systems no deuterium scrambling occurs. The Pd-phenyl product formed upon C–H activation is unstable, and biphenyl is formed as the final organic product. Pd(0) produced in the reaction is reoxidized to Pd(II) by O_2 (1 atm). Using toluene and α,α,α-trifluorotoluene as substrates results in biaryl formation with enriched *meta* and *para* substitution, respectively. Although a catalytic process remains elusive, the tandem C–H activation/O_2 activation sequence represents a promising step toward an aerobic oxidation of unactivated arenes to biaryls.

Experimental

General Considerations. All moisture-sensitive compounds were manipulated using standard vacuum line, Schlenk, or cannula techniques or in a drybox under a nitrogen atmosphere. Argon and dinitrogen gases were purified by passage over columns of MnO on vermiculite and activated molecular sieves. Trifluoroethanol was purchased from either Aldrich or Lancanster, purified and dried over a mixture of $CaSO_4/NaHCO_3$ then either vacuum distilled or distilled under argon, and stored over activated molecular sieves under vacuum. Trifluoroethanol-d_3 was purchased from Aldrich or Cambridge Isotopes, stored over activated molecular sieves and a small amount of $NaHCO_3$ under vacuum, then vacuum distilled. The solvent was syringed into oven-dried screw-cap NMR tubes fitted with septa for kinetic studies. Benzene and benzene-d_6 were vacuum distilled from sodium benzophenone ketyl shortly before kinetic runs, and stored over activated molecular sieves. Diethyl ether, THF, and CH_2Cl_2 were purified over an activated alumina column. 1,4-*Bis*(3,5-di-*tert*-butylphenyl)-2,3-dimethyl-1,4-diaza-1,3-butadiene ($^{tBu}{}_2{}^{Ar}DAB^{Me}$),[10a] 1,4-*bis*(3,5-di-trifluoromethylphenyl)-2,3-dimethyl-1,4-diaza-1,3-butadiene {$^{(CF_3)}{}_2{}^{Ar}DAB^{Me}$},[10b] [(COD)$PdMe_2$],[14] [(pyridazine)$PdMe_2$]$_n$,[13] ($^{tBu}{}_2{}^{Ar}DAB^{Me}$)$PdMe_2$ (**3a**),[11] {$^{(CF_3)}{}_2{}^{Ar}DAB^{Me}$}$PdMe_2$ (**3b**),[11] [($^{tBu}{}_2{}^{Ar}DAB^{Me}$)Pd($H_2O$)$_2$][$BF_4$]$_2$ (**4a**),[23] [($^{tBu}{}_2{}^{Ar}DAB^{Me}$)Pd(OH)]$_2$[$BF_4$]$_2$ (**5a**),[23] [$(PhCN)_2PdCl_2$],[31] and ($^{tBu}{}_2{}^{Ar}DAB^{Me}$)$PdCl_2$ (**6a**),[22] were synthesized according to literature procedures. All other solvents and reagents were used as received without further purification.

NMR spectra were recorded on a Varian CCE 600 (^{1}H, 599.662 MHz), a Varian INOVA 500 (^{1}H, 499.852 MHz) or a Varian Mercury 300 (^{1}H, 299.8 MHz, ^{19}F, 282.081 MHz, ^{13}C, 75.4626 MHz) spectrometer. Elemental analyses were performed at Midwest MicroLab LLC.

Synthesis and Characterization of Methyl Aquo Cations (2a/b). The aquo adducts of **3a/b** were prepared *in situ* by procedures described by Tilset and co-workers.[10b] Complexes **2a/b** could not be isolated as pure solids, but are stable in TFE solution for > 12 hours. For the kinetic studies, cations **2a/b** are generated *in situ* (vide infra), and the chemical shifts reported below are for solutions in TFE-d_3 in the absence of substrate.

[($^{tBu}_2$^{Ar}DAB^{Me})Pd(CH$_3$)(H$_2$O)][BF$_4$] (2a). ^{1}H NMR (300 MHz, TFE-d_3): δ = 0.492 (s, 3H, Pd-CH_3), 1.34, 1.36 (s, 18H, C(CH_3)$_3$), 2.12, 2.19 (s, 3H, N=C–CH_3), 6.77, 6.93 (d, $^4J_{H\text{-}H}$ = 1.6 Hz, 2H, *o*-Ar–*H*), 7.49, 7.55 (t, 1H, *p*-Ar–*H*).

[{(^{CF_3})$_2$^{Ar}DAB^{Me}}Pd(CH$_3$)(H$_2$O)][BF$_4$] (2b). ^{1}H NMR (600 MHz, TFE-d_3): δ = 0.511 (s, 3H, Pd-CH_3), 2.20, 2.28 (s, 3H, N=C–CH_3), 7.50, 7.58 (br s, 2H, *o*-Ar–*H*), 7.94, 7.95 (br s, 1H, *p*-Ar–*H*).

($^{tBu}_2$^{Ar}DAB^{Me})PdMe$_2$ (3a). A Schlenk flask was charged with [(pyridazine)PdMe$_2$]$_n$ (0.115 g, 0.530 mmol) and $^{tBu}_2$^{Ar}DAB^{Me} (0.256 g, 0.556 mmol). The flask was cooled to 0 ˚C, and Et$_2$O (15 mL) was transferred via cannula onto the solids. A dark red precipitate forms from the suspension of

starting materials almost immediately upon solvent addition. The mixture was stirred for 2 h at 0 ˚C, warmed to room temperature, and filtered. The crude product was dissolved in CH_2Cl_2 (3-4 mL); the resulting solution was filtered through Celite and concentrated in vacuo, affording **3a** as a red solid (0.199 g, 63%). ^{1}H NMR (300 MHz, CD_2Cl_2): δ = -0.269 (s, 6H, Pd-C*H*$_3$), 1.35 (s, 36H, C(C*H*$_3$)$_3$), 2.06 (s, 6H, N=C–C*H*$_3$), 6.73 (d, $^4J_{H-H}$ = 1.8 Hz, 4H, *o*-Ar-*H*), 7.28 (t, $^4J_{H-H}$ = 1.8 Hz, 2H, *p*-Ar-*H*). ^{13}C {^{1}H} NMR (300 MHz, CD_2Cl_2): δ = -5.189 (Pd-*C*H$_3$), 20.16 (N=C–*C*H$_3$), 31.73 (C(*C*H$_3$)$_3$), 35.50 (*C*(CH$_3$)$_3$), 115.76 (*o*-Ar-*C*), 119.64 (*p*-Ar-*C*), 147.34, 151.92 (Ar–*C*), 169.84 (N=*C*–CH$_3$). Anal. Calcd for $C_{34}H_{54}N_2Pd$ (Found): C, 68.38 (68.23/68.10); H, 9.11 (8.90/8.72); N, 4.69 (4.60/4.73).

{$^{(CF_3)_2Ar}$DAB^{Me}}PdMe$_2$ (3b). A Schlenk flask was charged with [(COD)PdMe$_2$ (0.122 g, 0.500 mmol) and $^{(CF_3)_2Ar}$DAB^{Me} (0.257 g, 0.500 mmol). The flask was cooled to 0 ˚C, and Et_2O (10 mL) was transferred via cannula onto the solids. A bright red precipitate formed from a clear solution, and the resulting red suspension was stirred for 1 h at 0 ˚C and warmed to room temperature. The red solid was filtered, washed with cold Et_2O and pentane, and dried in vacuo affording **3b** as a red powder (0.185 g, 58%). ^{1}H NMR (300 MHz, CD_2Cl_2): δ = -0.217 (s, 6H, Pd-C*H*$_3$), 2.11 (s, 6H, N=C–C*H*$_3$), 7.45 (br s, 4H, *o*-Ar-*H*), 7.84 (br s, 2H, *p*-Ar-*H*). ^{13}C {^{1}H} NMR (300 MHz, acetone-*d*$_6$): δ = -4.72 (Pd-*C*H$_3$), 20.59 (N=C–*C*H$_3$), 119.50 (m, $^3J_{C-F}$ = 3.8 Hz, *p*-Ar-*C*), 122.30 (m, $^3J_{C-F}$ = 3.8 Hz, *o*-Ar-*C*), 124.10 (q, $^1J_{C-F}$ = 273 Hz, *C*F$_3$), 132.15 (q, $^2J_{C-F}$ = 273 Hz, *m*-Ar-*C*-CF$_3$), 149.80 (Ar–*C*), 173.96 (N=*C*–CH$_3$). Anal. Calcd for $C_{22}H_{18}F_{12}N_2Pd$ (Found): C, 40.98

(41.18/41.13); H, 2.81 (2.91/2.92); N, 4.34 (4.24/4.27).

[($^{tBu}_2$^{Ar}DAB^{Me})Pd(H_2O)$_2$][BF_4]$_2$ (4a). ($^{tBu}_2$^{Ar}DAB^{Me})$PdCl_2$ (**6a**, 0.250 g, 0.392 mmol) was slurried in 1:1 THF/CH_2Cl_2 solution (15 mL). $AgBF_4$ (0.156 g, 0.803 mmol) was dissolved in dry THF (1 mL) and added to the reaction flask dropwise. An off-white precipitated formed immediately in a yellow solution. After 3 h, the solution was filtered through Celite and the filtrate is removed in vacuo to afford **4a** as a yellow solid (0.225 g, 74%). ^{1}H NMR (300 MHz, TFE-d_3): δ = 1.37 (s, 36H, C(CH_3)$_3$), 2.27 (s, 6H, N=C–CH_3), 7.23 (d, $^4J_{H\text{-}H}$ = 1.6 Hz, 4H, *o*-Ar-*H*), 7.77 (t, $^4J_{H\text{-}H}$ = 1.6 Hz, 2H, *p*-Ar–*H*), O–*H* resonances not found due to exchange with CF_3CD_2O**D**. ^{13}C {^{1}H} NMR (300 MHz, TFE-d_3): δ = 21.34 (N=C–*C*H_3), 31.99 (C(*C*H_3)$_3$), 37.01 (*C*(CH$_3$)$_3$), 118.42 (*o*-Ar-*C*), 127.17 (*p*-Ar-*C*), 143.91, 156.55 (Ar–*C*), 187.66 (N=*C*–CH$_3$). Anal. Calcd for $C_{32}H_{52}N_2O_2F_8B_2Pd$ (Found): C, 49.48 (49.18/49.17); H, 6.75 (6.68/6.73); N, 3.61 (3.59/3.55).

[{(CF_3)$_2$^{Ar}DAB^{Me}}Pd(H_2O)$_2$][BF_4]$_2$ (4b). ^{1}H NMR (600 MHz, TFE-d_3): δ = 2.19 (s, 6H, N=C–CH_3), 8.12 (br s, 4H, *o*-Ar-*H*), 8.18 (br s, 2H, *p*-Ar–*H*), O–*H* resonances not found due to exchange with CF_3CD_2O**D**.

[($^{tBu}_2$^{Ar}DAB^{Me})Pd(OH)]$_2$[BF_4]$_2$ (5a). This compound was synthesized in the same manner as **4a**, but is present in the solid isolated after a 1 h reaction time. This complex was not isolated cleanly from **4a** and other related products (see Results and Discussion Section), but can be isolated cleanly from the reaction of

2a with C_6H_6 (under 1 atm O_2). ^{1}H NMR (300 MHz, TFE-d_3): δ = 1.24 (s, 72H, C(CH_3)$_3$), 2.09 (s, 12H, N=C–CH_3), 6.87 (d, $^4J_{H\text{-}H}$ = 1.6 Hz, 8H, *o*-Ar-*H*), 7.52 (t, $^4J_{H\text{-}H}$ = 1.6 Hz, 4H, *p*-Ar–*H*), O–*H* resonances not found due to exchange with CF_3CD_2O**D**. ^{1}H NMR (300 MHz, CD_2Cl_2): δ = -3.51 (s, 2H, O*H*), 1.19 (s, 72H, C(CH_3)$_3$), 2.06 (s, 12H, N=C–CH_3), 6.93 (d, $^4J_{H\text{-}H}$ = 1.6 Hz, 8H, *o*-Ar-*H*), 7.34 (t, $^4J_{H\text{-}H}$ = 1.6 Hz, 4H, *p*-Ar–*H*).

[{$(CF_3)_2^{Ar}$DAB^{Me}}Pd(OH)]$_2$[BF_4]$_2$ (5b). ^{1}H NMR (600 MHz, TFE-d_3): δ = 1.99 (s, 12H, N=C–CH_3), 7.61 (br s, 8H, *o*-Ar-*H*), 8.01 (br s, 4H, *p*-Ar–*H*), O–*H* resonances not found due to exchange with CF_3CD_2O**D**.

($^{tBu}_2$^{Ar}DAB^{Me})PdCl$_2$ (6a). $^{tBu}_2$^{Ar}DAB^{Me} (0.520 g, 1.13 mmol) was dissolved in CH_2Cl_2 (10 mL) and added to a solution of [(PhCN)$_2$PdCl$_2$] (0.433 g, 1.13 mmol) in CH_2Cl_2 (10 mL). An orange precipitate formed immediately. The reaction was stirred for 1-2 h. The precipitate was filtered, washed with CH_3OH and Et_2O, and dried in vacuo to afford **6a** as an orange powder (0.529 g, 73%). Due to the very low solubility of this complex, NMR spectroscopic data could not be collected. Anal. Calcd for $C_{32}H_{48}N_2Cl_2Pd$ (Found): C, 60.24 (60.17/60.21); H, 7.58 (7.41/7.48); N, 4.39 (4.41/4.36).

Measurement of Kinetics for C–H Bond Activation of Benzene. Dry TFE-d_3 (~ 700 μL) was added via syringe to an oven-dried 5 mm thin-walled NMR tube containing approximately 0.0075 mmol of (α-diimine)PdMe$_2$ (**3a/b**). Aqueous

HBF_4 (48 wt%, 1 μl, 0.00765 mmol) was added, and the mixture was shaken to form a clear, yellow solution. A predetermined amount of D_2O was then added to the tube. A screw-cap fitted with a septum was then affixed to the tube. The tube was frozen at -78 ˚C, evacuated with a needle then backfilled with 1 atm O_2 (ultrahigh purity). After thawing, the mixture was analyzed by ^1H NMR to confirm clean conversion to aquo adducts **2a/b**. A predetermined amount of substrate was then added to the NMR tube, and after allowing the mixture to equilibrate to the preset temperature in the probe, disappearance of the starting material was monitored. (the same observed rate constants are obtained by monitoring the appearance of biphenyl). Probe temperatures were calibrated with a methanol standard and were maintained at ± 0.2 ˚C throughout data acquisition. The observed rate constants are calculated by curve fitting to the expression $I_t = I_f + (I_0\text{-}I_f) \times \exp(-k_{obs} \times t)$, where I_t is the integration of peak relative to the residual solvent peak, $CF_3C\mathbf{H}DOD$. The water concentration is calculated as follows: $[H_2O] = [(1\ \mu l \times 1.4\ g{\cdot}mL^{-1} \times 52\% + y\ \mu l \times 1\ g{\cdot}mL^{-1})/18\ g{\cdot}mol^{-1}/V\ (mL)]$, where 1.4 $g{\cdot}mL^{-1}$ is the density of the aqueous HBF_4 solution, 52% is the wt% of water in this aqueous solution, y is the amount of extra water added and 1 $g{\cdot}mL^{-1}$ is the density of water. The volume of the reaction mixture is determined as $V\ (mL) = 0.01384H - 0.006754$, where H is the solvent height in millimeters. Addition of a small amount of benzene (e.g., 15 μl) to TFE-d_3 shifts the resonances for the diimine backbone methyls by as much as 0.3 ppm, and can significantly affect shimming.

Appendix: Summary of C–H bond activation kinetic data and rate law derivation for Scheme 4. Details of the structure determination for complex **5b**.[32]

Summary of Benzene C–H Bond Activation Kinetic Data. In all cases, [Pd] is kept at 0.01 – 0.011 *M*; the observed rate constants have an uncertainty between 5 - 10% of the reported values and are the average of duplicate or triplicate experiments.

Table 1. Water Concentration Dependence.

Pd Complex	Substrate	T (˚C)	[substrate](*M*)	[H_2O] (*M*)	k_{obs} (x 10^4)
2a	C_6H_6	25	0.218	0.056	32.8
2a	C_6H_6	25	0.218	0.133	29.1
2a	C_6H_6	25	0.218	0.249	22.9
2a	C_6H_6	25	0.218	0.442	13.1
2a	C_6D_6	25	0.220	0.442	3.2
2a	C_6H_6	25	0.218	0.828	10.2
2a	C_6H_6	25	0.218	1.21	7.3
2a	C_6H_6	25	0.218	2.37	4.6
2a	C_6H_6	25	0.218	4.68	2.7
2b	C_6H_6	25	0.222	0.215	14.7
2b	C_6H_6	25	0.233	0.451	7.4
2b	C_6H_6	25	0.220	0.747	5.3

Table 2. Ionic Strength Experiments.

Pt Complex	Substrate	T (˚C)	Substrate (*M*)	[H_2O] (*M*)	NMe_4BF_4 (*M*)	k_{obs} (x 10^4)
2a	C_6H_6	25	0.218	0.442	--	13.1
2a	C_6H_6	25	0.218	0.442	0.10	13.0
2a	C_6H_6	25	0.218	0.828	--	10.2
2a	C_6H_6	25	0.218	0.828	0.10	9.6

Table 3. Temperature Dependence.

Pt Complex	Substrate	T (˚C)	[substrate](*M*)	[H_2O] (*M*)	k_{obs} (x 10^4)
2a	C_6H_6	1.1	0.218	0.442	0.43
2a	C_6H_6	25	0.218	0.442	13.1
2a	C_6H_6	41	0.218	0.442	53.9

Table 4. $[C_6H_6]$ Dependence.

Pt Complex	Substrate	T (˚C)	[substrate](*M*)	$[H_2O]$ (*M*)	k_{obs} (x 10^4)
2a	C_6H_6	25	0.109	0.442	7.1
2a	C_6H_6	25	0.218	0.442	13.1
2a	C_6H_6	25	0.435	0.442	24.7
2b	C_6H_6	25	0.111	0.451	2.5
2b	C_6H_6	25	0.233	0.451	7.4
2b	C_6H_6	25	0.435	0.451	13.3

Table 5. Substrate Dependence.

Pt Complex	Substrate	T (˚C)	[substrate](*M*)	$[H_2O]$ (*M*)	k_{obs} (x 10^4)
2a	C_6H_6	25	0.218	0.442	13.1
2a	$C_6H_5CH_3$	25	0.217	0.442	26.8
2a	$C_6H_5CF_3$	25	0.220	0.449	1.1

Rate Law Derivation

$$\text{Define } [\text{Pd}]_T = [\mathbf{A}i] + [\mathbf{A}ii] \qquad K_{eq} = \frac{[\mathbf{A}ii][\text{TFE}]}{[\mathbf{A}i][\text{H}_2\text{O}]}$$

$$\text{Then } [\text{Pd}]_T = [\mathbf{A}i]\left[1 + \frac{K_{eq}[\text{H}_2\text{O}]}{[\text{TFE}]}\right]; \quad [\mathbf{A}i] = \frac{[\text{Pd}]_T}{1 + \frac{K_{eq}[\text{H}_2\text{O}]}{[\text{TFE}]}}$$

$$-\frac{d[\text{Pd}]_T}{d\text{t}} = k_2[\mathbf{B}]$$

Applying the steady-state approximation on [**B**]

$$\frac{d[\mathbf{B}]}{d\text{t}} = k_1[\mathbf{A}i][\text{C}_6\text{H}_6] - k_{-1}[\mathbf{B}][\text{TFE}] - k_2[\mathbf{B}] \cong 0$$

$$[\mathbf{B}] = \frac{k_1[\mathbf{A}i][\text{C}_6\text{H}_6]}{k_{-1}[\text{TFE}] + k_2}$$

$$-\frac{d[\text{Pd}]_T}{d\text{t}} = k_2 \cdot \frac{k_1[\text{C}_6\text{H}_6]}{k_{-1}[\text{TFE}] + k_2} \cdot \frac{[\text{Pd}]_T}{1 + \frac{K_{eq}[\text{H}_2\text{O}]}{[\text{TFE}]}}$$

$$= k_{obs}[\text{Pd}]_T = \frac{k_2}{k_{-1}[\text{TFE}] + k_2} \cdot \frac{k_1[\text{TFE}][\text{C}_6\text{H}_6][\text{Pd}]_T}{[\text{TFE}] + K_{eq}[\text{H}_2\text{O}]}$$

Expression for $1/k_{obs}$ vs. $[H_2O]/[C_6H_6]$ plot:

$$\frac{1}{k_{\text{obs}}} = \frac{k_{-1}[\text{TFE}] + k_2}{k_2} \cdot \frac{[\text{TFE}] + K_{eq}[H_2O]}{k_1[\text{TFE}][C_6H_6]}$$

$$= \underbrace{\frac{k_{-1}[\text{TFE}] + k_2}{k_2} \cdot \frac{K_{eq}[H_2O]}{k_1[\text{TFE}][C_6H_6]}} + \underbrace{\frac{k_{-1}[\text{TFE}] + k_2}{k_2} \cdot \frac{[\text{TFE}]}{k_1[\text{TFE}][C_6H_6]}}$$

$$\text{slope} = \frac{k_{-1}[\text{TFE}] + k_2}{k_2} \cdot \frac{K_{eq}}{k_1[\text{TFE}]} \qquad \text{intercept} = \frac{k_{-1}[\text{TFE}] + k_2}{k_2} \cdot \frac{1}{k_1[C_6H_6]}$$

$$\frac{\text{intercept}}{\text{slope}} = \frac{1}{k_1[C_6H_6]} \cdot \frac{k_1[\text{TFE}]}{K_{eq}} = \frac{[\text{TFE}]}{K_{eq}[C_6H_6]}$$

K_{eq} calculated indirectly by this method

Crystallography: Crystal data, intensity collection, and refinement details are presented in Table 6 for compound **5b**.

Data Collection and Processing: Data for compound **5b** was collected on a Bruker SMART 1000 area detector running SMART.[33] The diffractometer was equipped with a Crystal Logic CL24 low temperature device and all datasets were collected at low temperature. The diffractometer used graphite-monochromated MoKα radiation with λ = 0.71073 Å.

The crystal was mounted on a glass fiber with Paratone-N oil. Data were collected as ω–scans at seven values of φ. The detector was 5 cm (nominal) distant at a θ of –28°. The data were processed with SAINT.[31]

Table 6. X-ray Experimental Data.

Compound	**5b**
formula	$C_{40}H_{24}B_2F_{32}N_4O_2Pd_2$
formula weight	1435.05
crystal system	monoclinic
space group	$P2_1$
a, Å	15.7429(7)
b, Å	10.3772(5)
c, Å	15.8713(7)
α, °	90
β, °	108.1380(10)

γ, °	90
volume, Å^3	2464.01(19)
Z	2
ρ_{calc}, g/cm^3	1.934
μ, mm^{-1}	0.89
F_{000}	1396
crystal shape	plate
crystal color	yellow
crystal size, mm	0.26 x 0.14 x 0.09
T, K	98
type of diffractometer	SMART 1000 ccd
θ range, °	1.59, 28.44
h,k,l limits	-20, 20; -13, 13; -21, 20
data measured	50764
unique data	11439
data, $F_o>4\sigma(F_o)$	11439
parameters / restraints	743/1
R1[a],wR2[b]; all data	0.0403, 0.0686
R1[a],wR2[b]; $F_o>4\sigma(F_o)$	0.0352, 0.0679
GOF[c] on F^2	1.98
$\Delta\rho_{max,min}$, e·Å^{-3}	1.004, -0.683

All data were collected with graphite monochromated MoKα radiation (λ=0.71073 Å).

[a] $R1 = \Sigma \, | \, |F_o| - |F_c| \, | \, / \, \Sigma \, |F_o|$

[b] $wR2 = \{ \, \Sigma[w(F_o^2 - F_c^2)^2] \, / \, \Sigma[w(F_o^2)^2] \, \}^{1/2}$

[c] $GOF = S = \{ \, \Sigma[w(F_o^2 - F_c^2)^2] \, / \, (n-p) \, \}^{1/2}$

Structure analysis and refinement: SHELXTL v5.1 was used to solve, via direct methods, and to refine all structures using full-matrix least-squares. All non-hydrogen atoms were refined anisotropically. All hydrogen atoms were refined isotropically.

References

(1) (a) Labinger, J. A.; Bercaw, J. E. *Nature* **2002**, *417*, 507-514. (b) Jia, C.; Kitamura, T.; Fujiwara, Y. *Acc. Chem. Res.* **2001**, *34*, 633-639. (c) Crabtree, R. H. *J. Chem. Soc., Dalton Trans.* **2001**, 2437-2450. (d) Shilov, A. E., Shul'pin, G. B. *Chem. Rev.* **1997**, *97*, 2879-2932. (e) Arndtsen, B. A.; Bergman, R. G.; Mobley, T. A.; Peterson, T. H. *Acc. Chem. Res.* **1995**, *28*, 154-162. (f) *Selective Hydrocarbon Activation*; Davies, J. A.; Watson, P. L.; Liebman, J. F. and Greenberg, A., Eds.; VCH: New York, 1990. (g) *Activation and Functionalization of Alkanes*; Hill, C. L., Ed.; John Wiley & Sons: New York, 1989. (h) Shilov, A. E.; Shul'pin, G. B. *Activation and Catalytic Reactions of Saturated Hydrocarbons in the Presence of Metal Complexes.* Kluwer Academic Publishers: Dordrecht, 2000.

(2) Gol'dshleger, N. F.; Es'kova, V. V.; Shilov, A. E.; Shteinman, A. A. *Zh. Fiz. Khim.* **1972**, *46*, 1353–1354 (English translation **1972**, *46*, 785–786).

(3) Stahl, S. S.; Labinger, J. A.; Bercaw, J. E. *Angew. Chem., Int. Ed.* **1998**, *37*, 2181–2192 and references therein.

(4) (a) Rostovtsev, V. V.; Henling, L. M.; Labinger, J. A.; Bercaw, J. E. *Inorg. Chem*. **2002**, *41*, 3608-3619. (b) Scollard J. D.; Day M.; Labinger J. A.; Bercaw, J. E. *Helv. Chim. Acta* **2001**, *84*, 3247-3268.

(5) (a) Jintoku, T.; Taniguchi, H.; Fujiwara, Y. *Chem. Lett.* **1987**, 1865-1868. (b) Jintoku, T.; Takaki, K.; Fujiwara, Y.; Fuchita, Y.; Hiraki, K. *Bull. Chem. Soc. Jpn.* **1990**, *63*, 438-441.

(6) (a) ten Brink, G. J.; Arends, I. W. C. E.; Sheldon, R. A. *Science* **2000**, *287*, 1636-1639. (b) Nishimura, T.; Onoue, T.; Ohe, K.; Uemura, S. *J. Org. Chem.* **1999**, *64*, 6750-6755. (c) Peterson, K. P.; Larock, R. C. *J. Org. Chem.* **1998**, *63*, 3185-3189. For

enantioselective oxidations: (d) Jensen, D. R.; Pugsley, J. S.; Sigman, M. S. *J. Am. Chem. Soc.* **2001**, *123*, 7475-7476. (e) Ferreira, E. M.; Stoltz, B. M. *J. Am. Chem. Soc.* **2001**, *123*, 7725-7726.

(7) Stahl, S. S.; Thorman, J. L.; Nelson, R. C.; Kozee, M. A. *J. Am. Chem. Soc.* **2001**, *123*, 7188-7189.

(8) Steinhoff, B. A.; Fix, S. R.; Stahl, S.S. *J. Am. Chem. Soc.* **2002**, *124*, 766-767 and references therein.

(9) Periana, R. A.; Taube, D. J.; Evitt, E. R.; Löffler, D. G.; Wentrcek, P. R.; Voss, G.; Masuda, T. *Science* **1993**, *259*, 340–343.

(10) (a) Zhong, H. A.; Labinger, J. A.; Bercaw, J. E. *J. Am. Chem. Soc.* **2002**, *124*, 1378-1399. (b) Johansson, L.; Ryan, O. B.; Tilset, M. *J. Am. Chem. Soc.* **1999**, *121*, 1974-1975. (c) Johansson., L.; Tilset, M.; Labinger, J. A.; Bercaw, J. E. *J. Am. Chem. Soc.* **2000**, *122*, 10846-10855.

(11) Tempel, D. J.; Johnson, L. K.; Huff, R. L.; White, P. S.; Brookhart, M. *J. Am. Chem. Soc*. **2000**, *122*, 6686-6700.

(12) Fang, X.; Scott, B. L.; Watkin, J. G.; Kubas, G. J. *Organometallics* **2000**, *19,* 4193-4195.

(13) Byers, P. K.; Canty, A. J. *Organometallics* **1990**, *9,* 210-220.

(14) Rudler-Chauvin, M.; Rudler, H. *J. Organomet. Chem.* **1977**, *134*, 115-119.

(15) In the original Pt work,[10a] the [D_2O] dependence studies were conducted at 293 K. The data for **1a** in Figure 1 have been calculated using Eyring data for comparison to [D_2O] studies for **2a/b** which were conducted at 298 K.

(16) The reported $\Delta S^{\ddagger}$ = 5 e.u. for **1a**[10a] was miscalculated. The correct value is $\Delta S^{\ddagger}$ = - 5 e.u.

(17) Plots of $1/k_{obs}$ vs $[C_6D_6]/[D_2O]$ extrapolated to zero $[D_2O]$ indicate that the palladium complex **2a** reacts with benzene faster than the platinum complex **1a** by a factor of approximately two.

(18) (a) Wick, D. D.; Goldberg, K. I. *J. Am. Chem. Soc.* **1997**, *119*, 10235-10236. (b) Reinartz S.; White P. S.; Brookhart M.; Templeton J. L. *J. Am. Chem. Soc.* **2001**, *123*, 12724-12725.

(19) Canty, A. J. *Acc. Chem. Res.* **1992**, *25*, 83-90 and references therein.

(20) The quantification of **5a/b** was accomplished by ^{1}H NMR integration against the residual solvent peak ($CF_3C\mathbf{H}DOD$) as an internal standard. The biphenyl quantification was accomplished by GC-MS.

(21) Attempts at catalytic C–C bond formation using either **4a** or **5a** gave only substoichiometric biphenyl; the bridged hydroxo and bis aquo complexes are apparently too inert to activate C–H bonds.

(22) van Asselt, R.; Elsevier, C. J.; Amatore, C.; Jutand, A. *Organometallics* **1997**, *16*, 317-328.

(23) Kannan, S.; James, A. J.; Sharp, P. R. *Polyhedron* **2000**, *19*, 153-163.

(24) Wimmer, S.; Castan, P.; Wimmer, F. L.; Johnson, N. P. *J. Chem. Soc. Dalton Trans.* **1989**, 403-412.

(25) Fujii, A.; Hagiwara, E.; Sodeoka, M. *J. Am. Chem. Soc.* **1999**, *121*, 5450-5458.

(26) Yagyu, T.; Hamada, M.; Osakada, K.; Yamamoto, T. *Organometallics* **2001**, *20*, 1087-1101 and references therein.

(27) Konze, W. V.; Scott, B. L.; Kubas, G. J. *J. Am. Chem. Soc.* **2002**, *124*, 12550-12556.

(28) Thomas, J. C.; Peters, J. P. *J. Am. Chem. Soc.*, *in press*.

(29) Littke, A. F.; Dai, C.; Fu., G. C. *J. Am. Chem. Soc.* **2000**, *122*, 4020-4028.

(30) Inoue, A.; Kitagawa, K.; Shinokubo, H.; Oshima, K. *Tetrahedron* **2000**, *56*, 9601-9605.

(31) Kharasch, M. S.; Seyler, R. C.; Mayo, F. R. *J. Am. Chem. Soc.* **1938**, *60*, 882-884.

(32) Crystallographic data for **5b** (CCDC 204983) have been deposited with the Cambridge Crystallographic Data Centre as supplementary publications. These data can be obtained free of charge via http://www.ccdc.cam.ac.uk/conts/retrieving.html (or from the Cambridge Crystallographic Data Centre, 12 Union Road, Cambridge CB2 1EZ, UK; fax: +44 1223 336033; or deposit@ccdc.cam.ac.uk). Structure factors are available electronically: e-mail: xray@caltech.edu.

(33) Bruker (1999) SMART, SAINT, and SHELXTL. Bruker AXS Inc., Madison, Wisconsin, USA.